# Characterization of biomaterials and biological materials: a toolbox

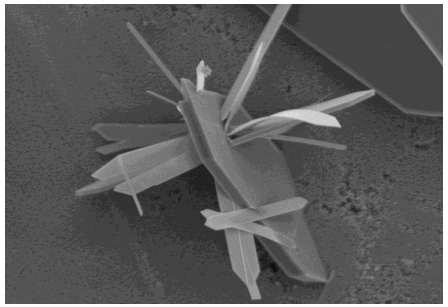

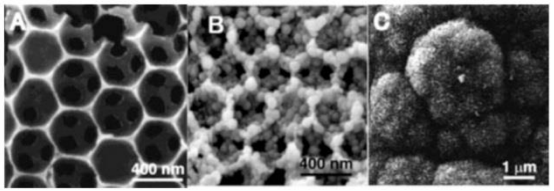


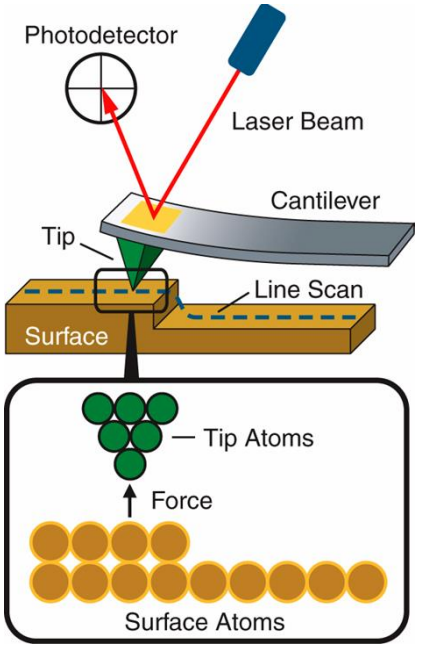


**C. Bonhomme – Professor in Chemistry**

**Laboratoire de Chimie de la Matière Condensée**

**UMR CNRS 7574 – Sorbonne Université, Paris**

**christian.bonhomme@upmc.fr**

# A specific class of materials

**bio-nanocomposites involving:**

- **minerals (hydroxyapatite $Ca_{10}(PO_4)_6(OH)_2$, calcium carbonate $CaCO_3$, calcium oxalates $CaC_2O_4.nH_2O$…) → eventual polymorphism**

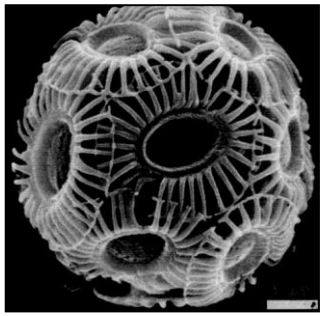

**calcite ($CaCO_3$)**

**… aragonite, vaterite**

- **organics (proteins…)**
- **organic/inorganic «interfaces»**

**intrinsic structural complexity**

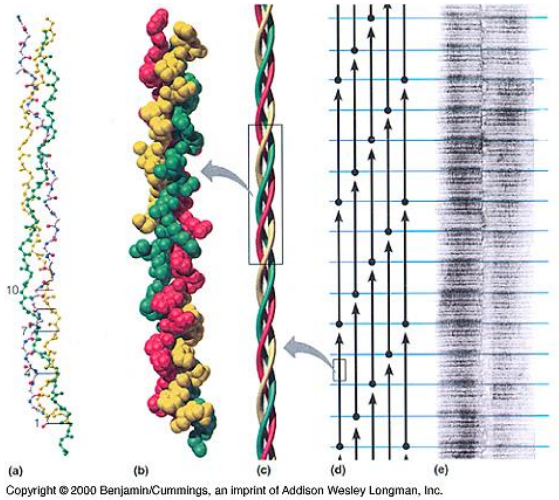



**collagen**

**multiple tools of investigation !**

# Hierarchical materials: from atomic (Å) to macroscopic (cm) description

## pathological calcifications (kidney stones)

**a major societal/health problem worldwide**

**(in France, related costs *per year*: > 800 millions $)**

- **minerals (calcium oxalates, phosphates, struvite…)**
- **proteins**
- **triglycerids**
- **…**

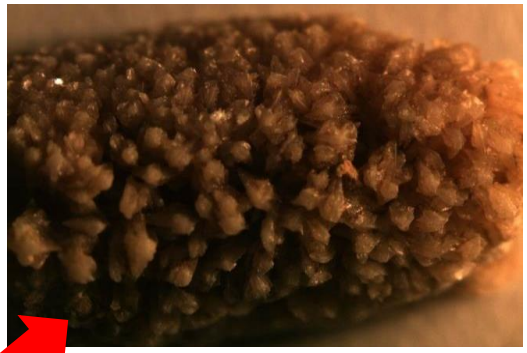

macro–scale

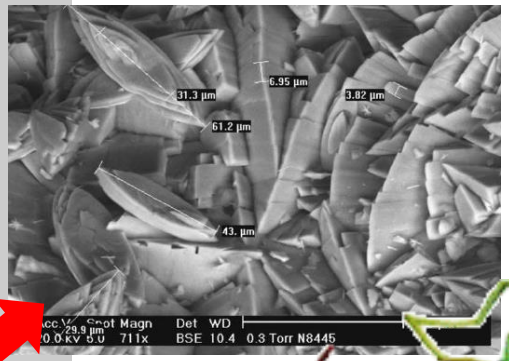


meso–

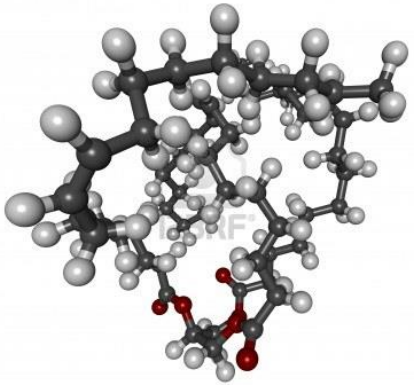

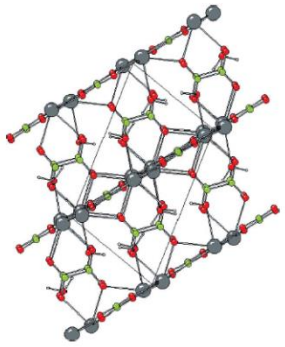

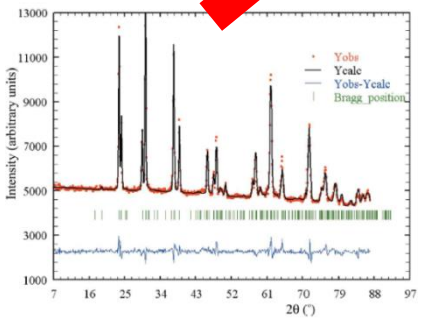


nano–

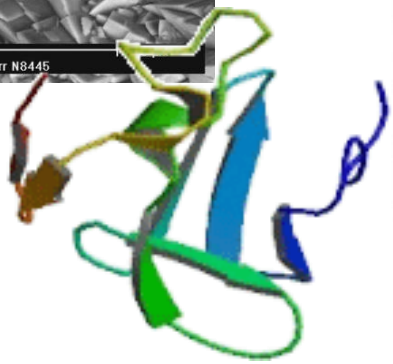

M. Daudon, D. Bazin *et al.*, *J. Appl. Crystallogr.*, 42,109–2009

# The electromagnetic spectrum

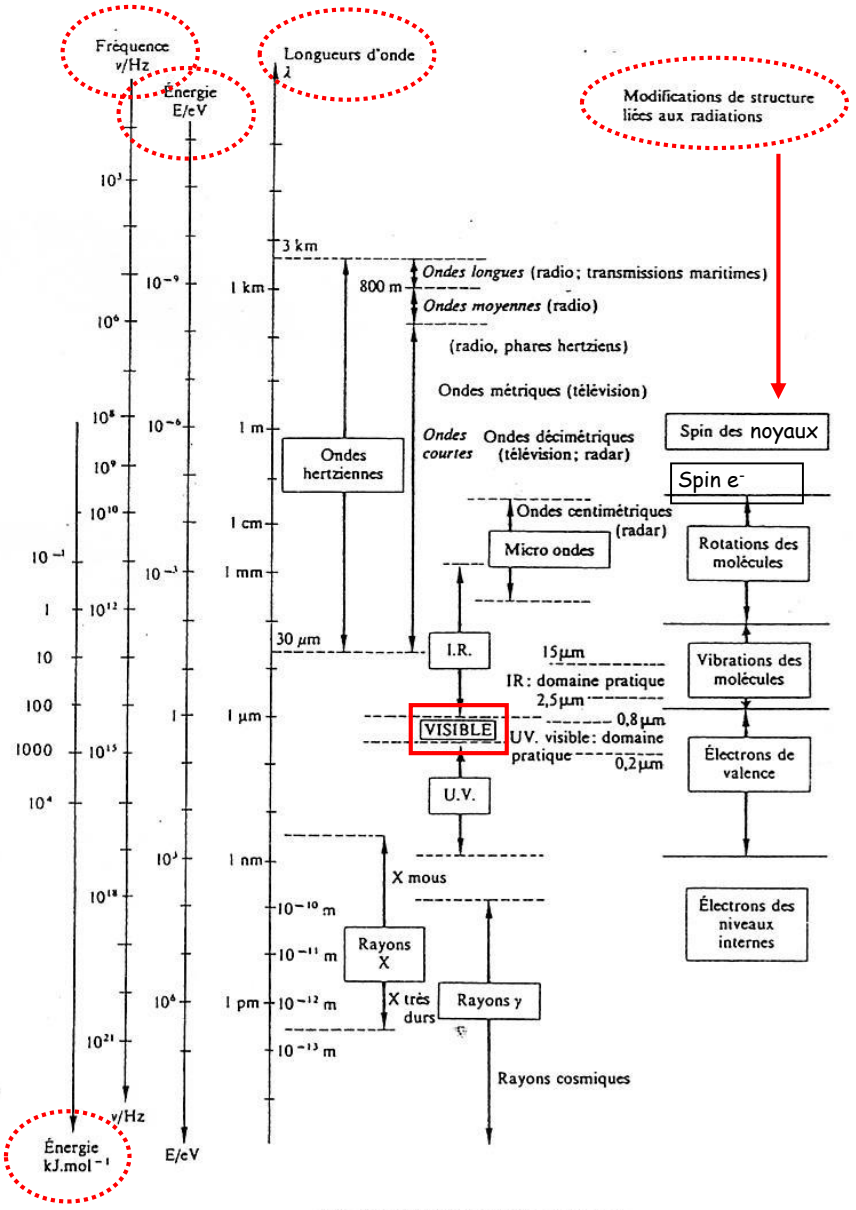


*Les radiations électromagnétiques.*

## keywords / questioning:

- local *vs* long range probe
- specific frequency / time domain
- complementarity of techniques
- advantages / drawbacks
- equipment (lab., synchrotron…)
- spectroscopy / diffraction / imaging

# Vibrational spectroscopies (IR and Raman diffusion)

## harmonic oscillator

$- \hbar^2/2m \, d^2\Psi/dx^2 + V(x)\Psi = E\,\Psi$

$V(x) = \frac{1}{2}\, kx^2$

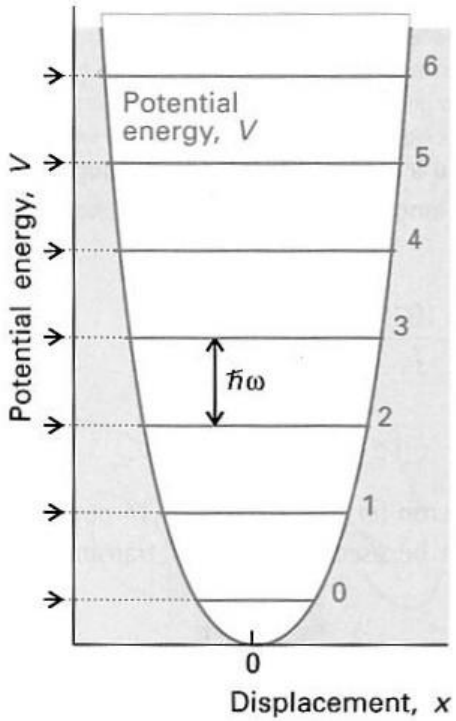


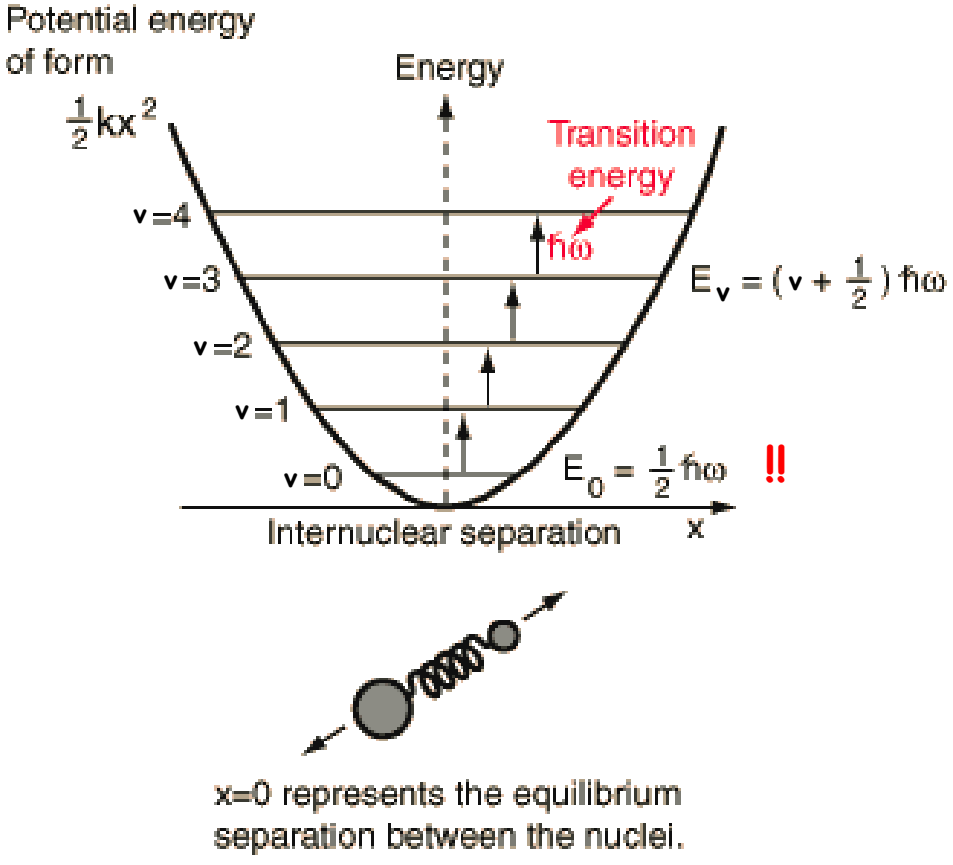




x=0 represents the equilibrium separation between the nuclei.

$E_v = (v+1/2)\hbar\omega \qquad \omega = (k/m)^{1/2}$

$\omega = (k/\mu)^{1/2}$

k : force constant

$\mu = m_1 m_2/(m_1+m_2)$

# Assignments of IR / Raman modes

**normal modes of vibrations**

**ex : $H_2O$**

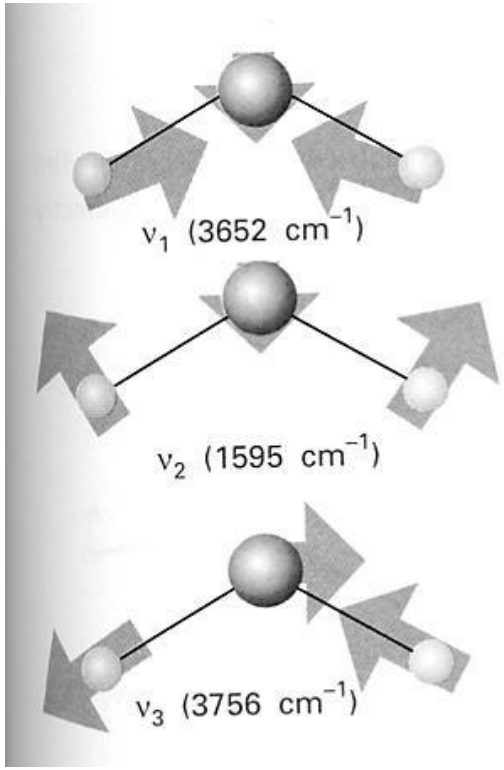


**characteristic frequencies**

| $\tilde{\nu}$/cm$^{-1}$ | |
|---|---|
| C—H stretch | 2850–2960 |
| C—H bend | 1340–1465 |
| C—C stretch | 700–1250 |
| C=C stretch | 1620–1680 |

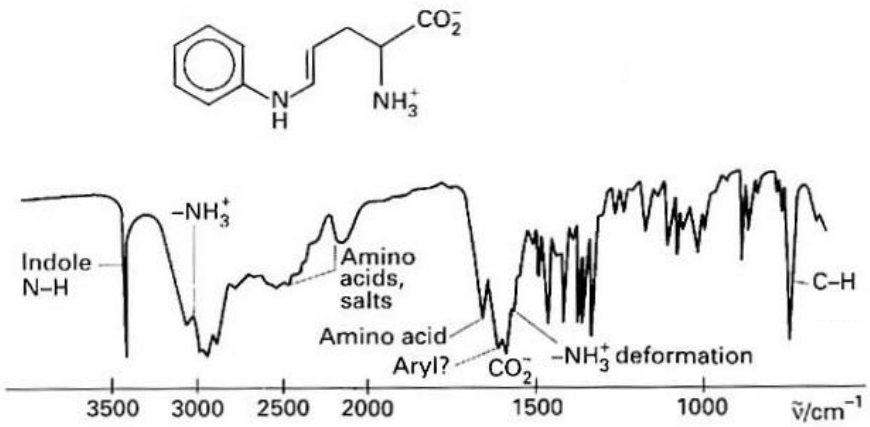


**symmetry**

**group theory**

**active / inactive modes (IR & Raman)**

# Hydroxyapatite, $Ca_{10}(PO_4)_6(OH)_2$ and carbonates

**main mineral in bones, teeth, enamel**

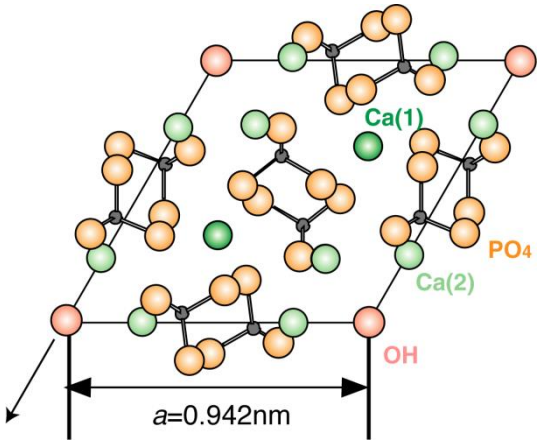


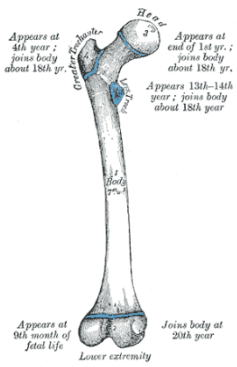

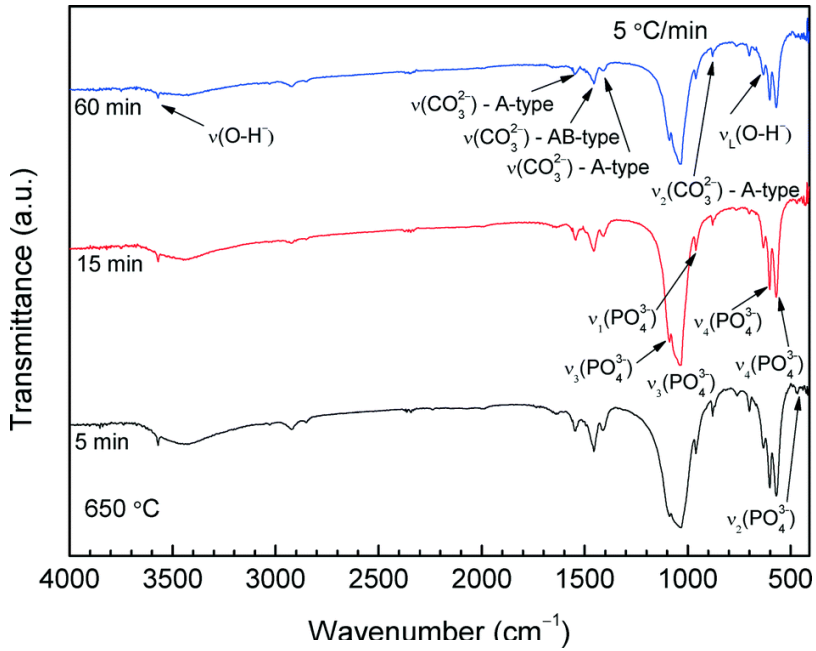


Edita Garskaite,*[a] Karlis-Agris Gross,*[b] Sung-Wei Yang,[c] Thomas Chung-Kuang Yang,[c] Jen-Chang Yang[d] and Aivaras Kareiva[e]

Show Affiliations

*CrystEngComm*, 2014, **16**, 3950-3959

$Ca_{10}(PO4)6(OH)2$

$Mg^{2+}$, $Zn^{2+}$, $Na^{+}$, $K^{+}$ …

$SO_4^{2-}$, $CO_3^{2-}$….

$CO_3^{2-}$, $F^{-}$, $Cl^{-}$…

$Ca_{10}(PO_4)_6(OH)_2$

B A

$SiO_4^{4-}$ $CO_3^{2-}$

# Nuclear Magnetic Resonance (NMR)

$\hat{\mu} = \gamma \hbar \hat{I}$

magnetic moment

spin angular momentum

gyromagnetic ratio

$E = - \mu . B$

Boltzmann equation

Curie's law

$$M = \frac{N \gamma^2 h^2 B_0 I(I+1)}{12 \pi^2 kT}$$

M

$B_0$ (~10T)


$m_I = -1/2$

$m_I = +1/2$

$\Delta m_I = \pm 1$

$\nu_0 = \gamma B_0 / 2\pi$

Larmor frequency !

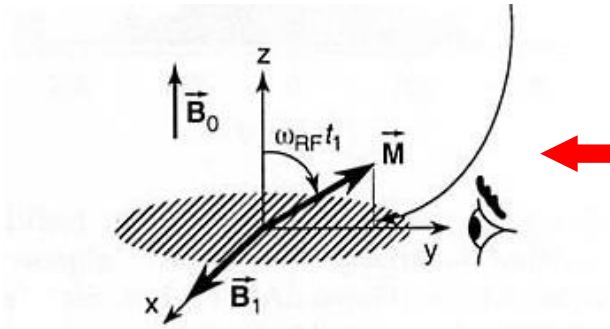


$M_y$

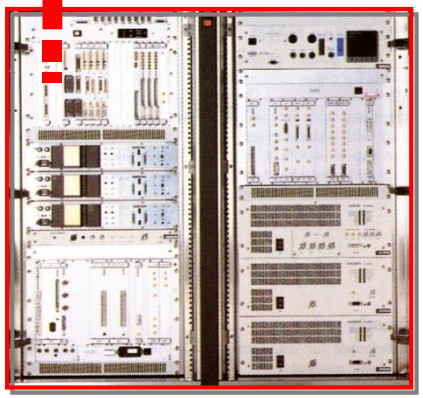

$B_1$ (RF) at resonance !

Man, Encyclopedia of analytical chemistry, 2000, 12228.

# NMR parameters: the chemical shift and J coupling

## interactions

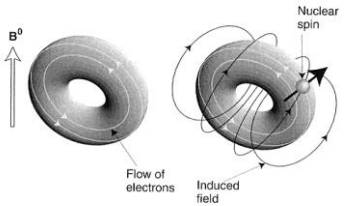


chemical shift: δ

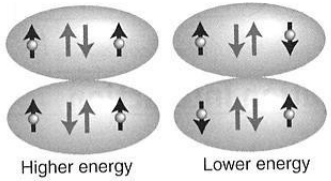


indirect coupling: J

$^{13}C$-{$^{1}H$}: the case of a steroid

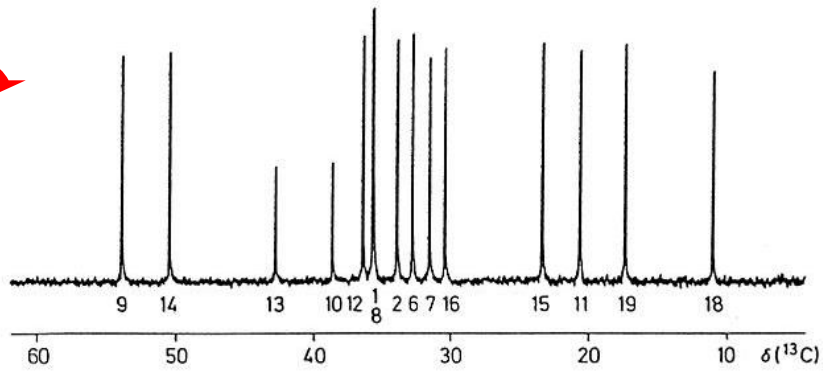


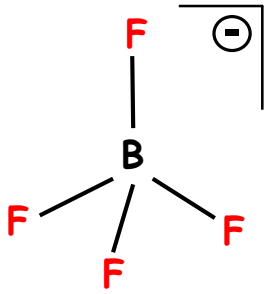


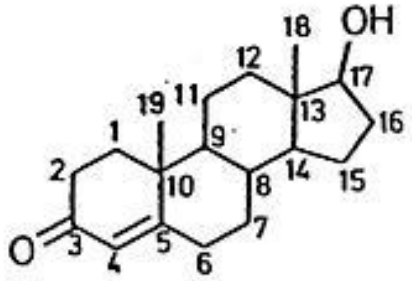


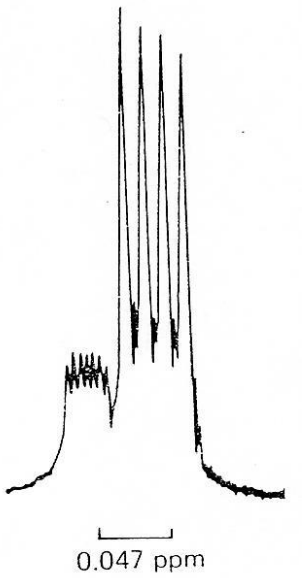


ex: $^{19}F$ spectrum of $BF_4^-$

multiplets (J in Hz)
δ in ppm

# Characterization of hydrated calcium oxalates by $^{13}C$ solid state NMR

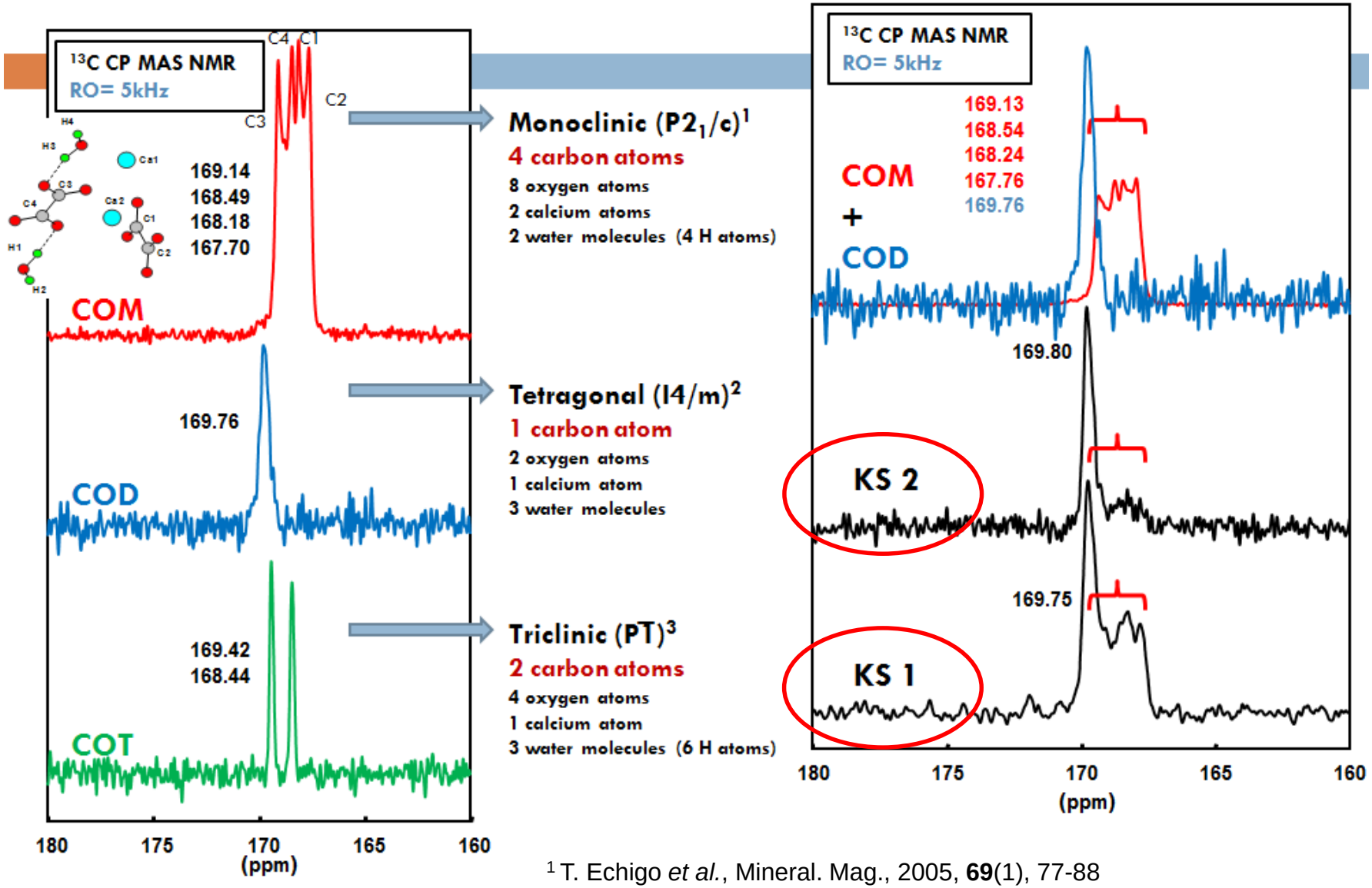


C. Leroy, PhD thesis

[1] T. Echigo *et al.*, Mineral. Mag., 2005, **69**(1), 77-88
[2] V. Tazzoli *et al.*, Amer. Mineral., 1980, **65**, 327-334
[3] S. Deganello *et al.*, Amer. Mineral., 1981, **66**, 859-865

# The structure of interfaces in biological hydroxyapatites

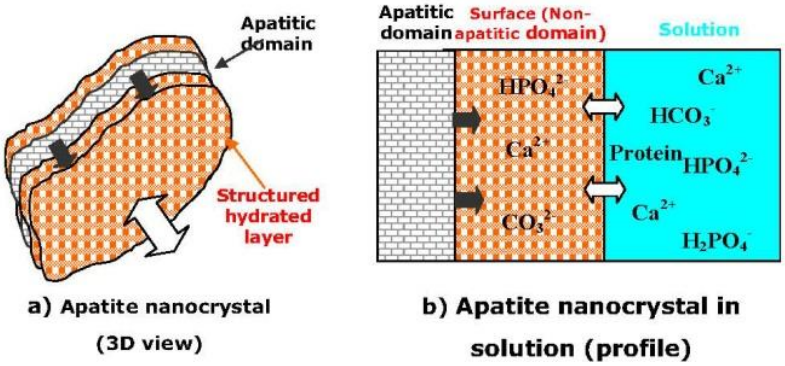


a model by C. Rey *et al.*, Toulouse

- 2D and 3D experiments
- connectivities and internuclear distances
- towards interfaces !

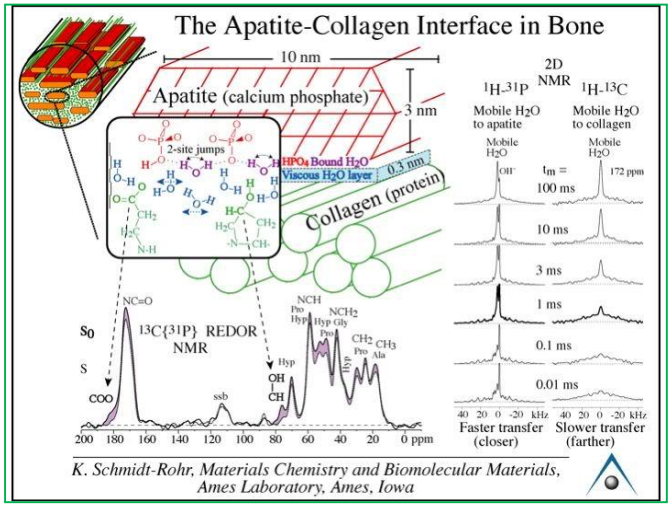


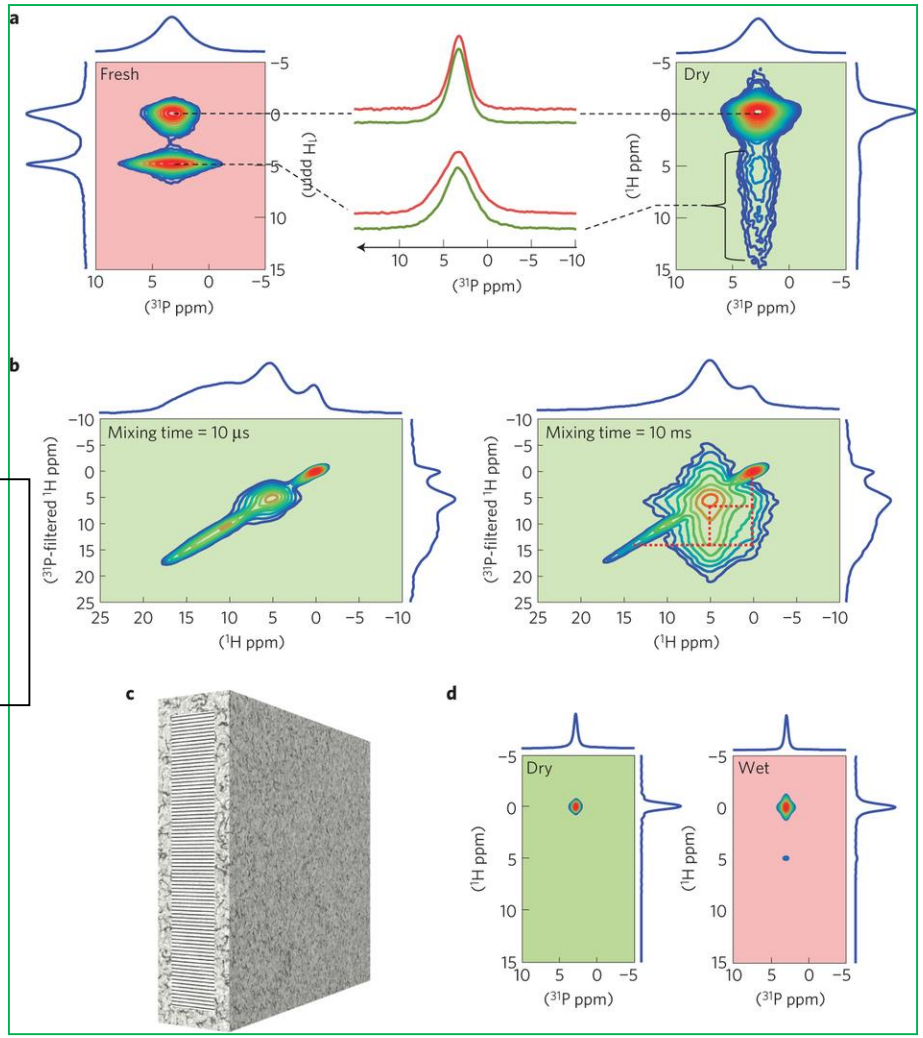


Y. Wang *et al.*, Nature Mater. 2013

# Imaging by NMR

## Phosphorus-31 MRI of hard and soft solids using quadratic echo line-narrowing

Merideth A. Frey[a], Michael Michaud[b], Joshua N. VanHouten[c], Karl L. Insogna[c], Joseph A. Madri[b], and Sean E. Barrett[a,1]

[a]Department of Physics, Yale University, New Haven, CT 06511; [b]Department of Pathology, School of Medicine, Yale University, New Haven, CT 06510; and [c]Department of Internal Medicine (Endocrinology), School of Medicine, Yale University, New Haven, CT 06510

Edited by Charles P. Slichter, University of Illinois at Urbana-Champaign, Urbana, IL, and approved January 28, 2012 (received for review October 20, 2011)

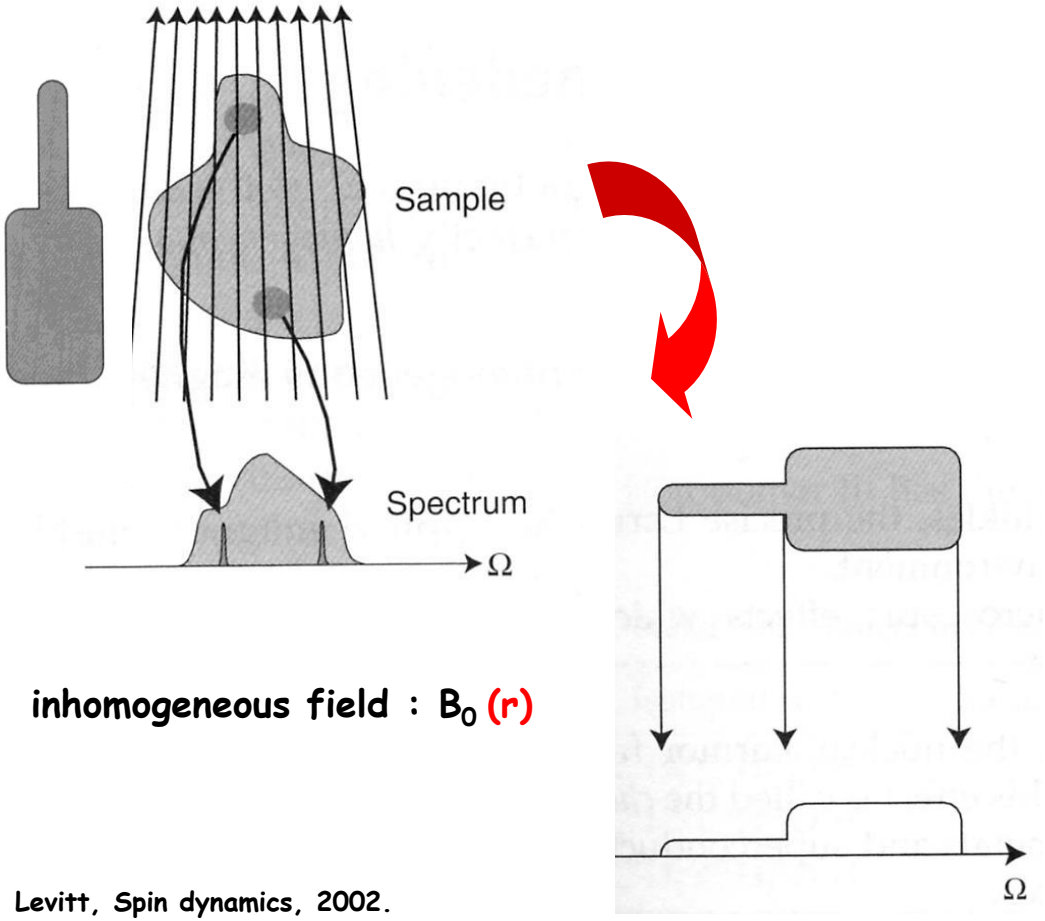


**inhomogeneous field : $B_0$ (r)**

Levitt, Spin dynamics, 2002.

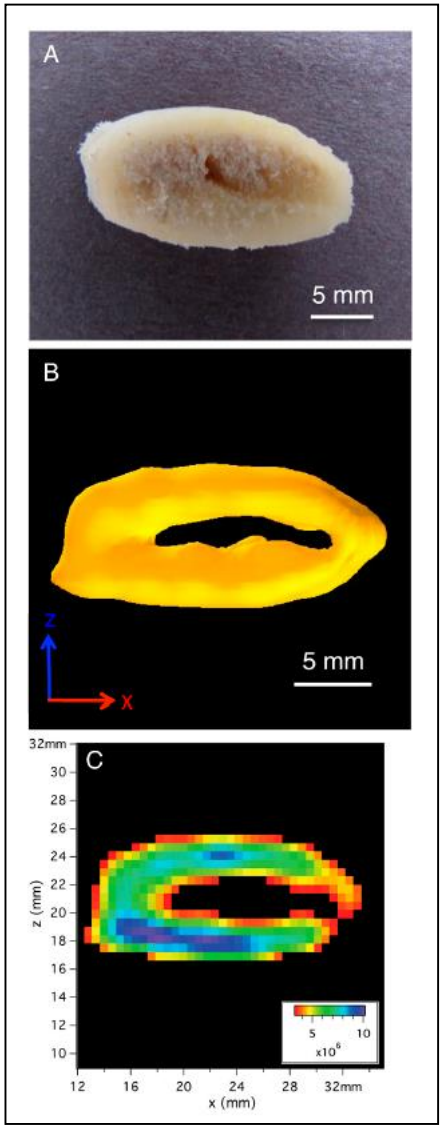


***ex vivo* bone sample**

# X-ray diffraction

## Thomson's formula (1856-1940)

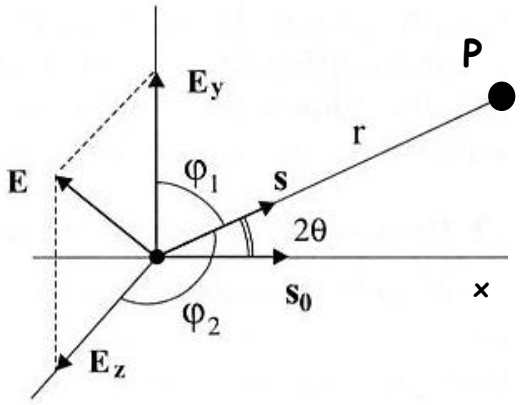


$$\frac{I_{diffusé}}{I_{incident}} = \left(\frac{\mu_0}{4\pi}\right)^2 \frac{e^4}{m^2 r^2} \frac{1+\cos^2 2\theta}{2}$$

as $m_p >> m_e$: only the contribution of the electrons has to be taken into account

## periodic crystalline structure

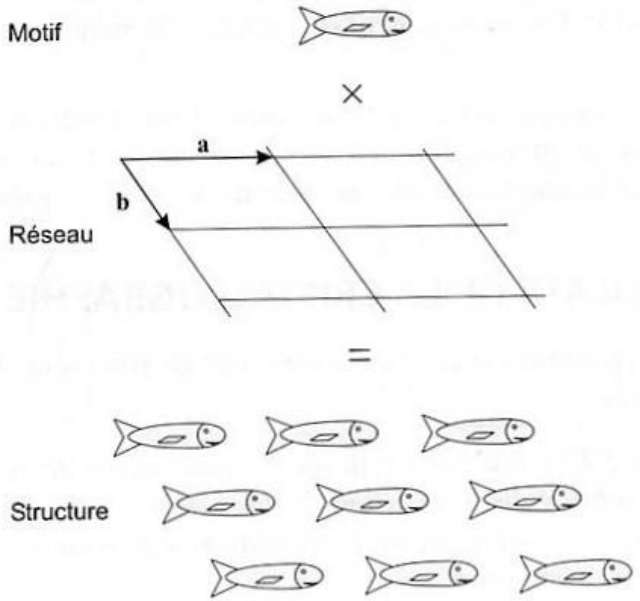


symmetry

cell

space group

# X-ray structure and powder pattern

periodic structure -> diffraction pattern !

"chemistry" × "periodicity"

electronic density calculation

powder diffraction

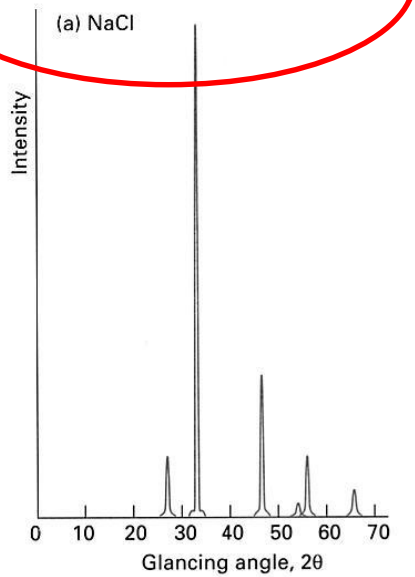


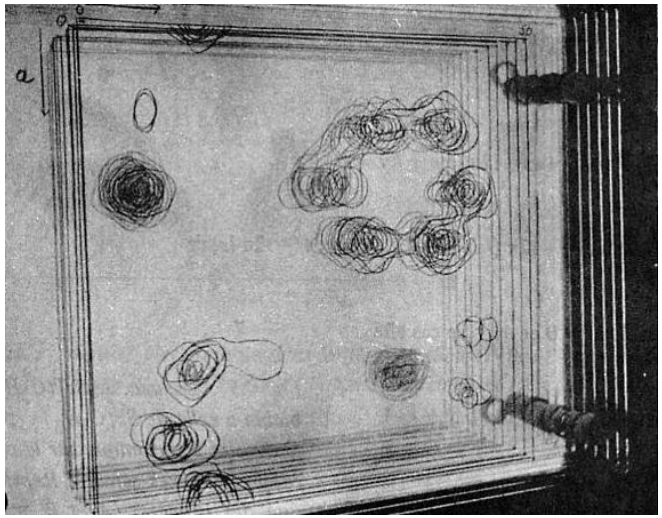

an old presentation: $LiCl.C_5H_5N$

single crystal diffraction

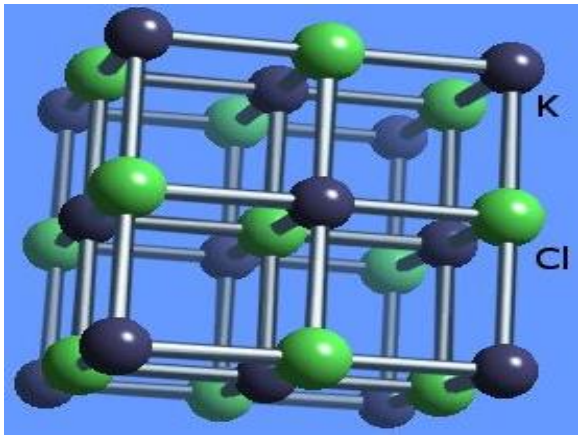


... to proteins !...

# X-ray diffraction: the case of $Cl^-$ substituted hydroxyapatite

Klemme *et al. Chemistry Central Journal* 2013, **7**:56
http://journal.chemistrycentral.com/content/7/1/56

Chemistry Central Journal

RESEARCH ARTICLE Open Access

## Synthesis of trace element bearing single crystals of Chlor-Apatite ($Ca_5(PO_4)_3Cl$) using the flux growth method

Stephan Klemme*, Timm John, Mathias Wessels, Christof Kusebauch, Jasper Berndt, Arno Rohrbach and Peter Schmid-Beurmann

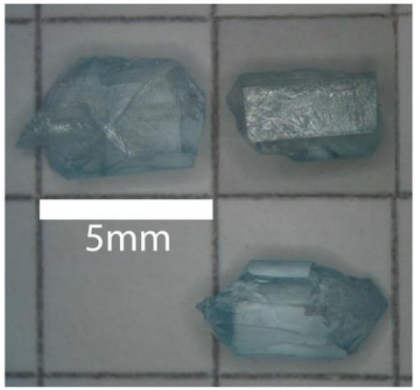


**Figure 1** Chlorapatite crystals grown with the flux method; crystals from experiment SynCLAP6.

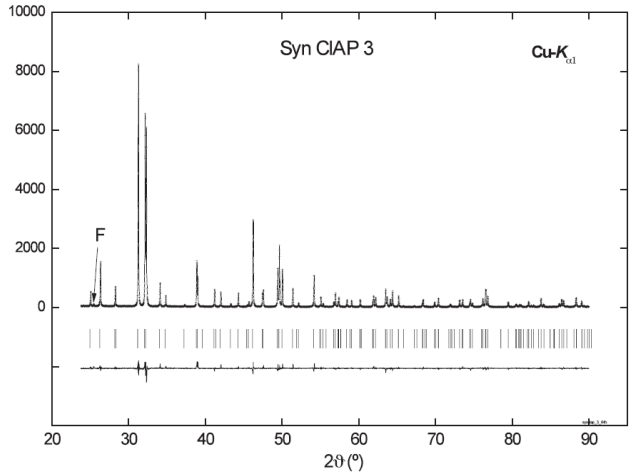


**Figure 2** X-ray diffraction: Observed, calculated and difference intensity powder patterns of synthetic chlor-apatite.

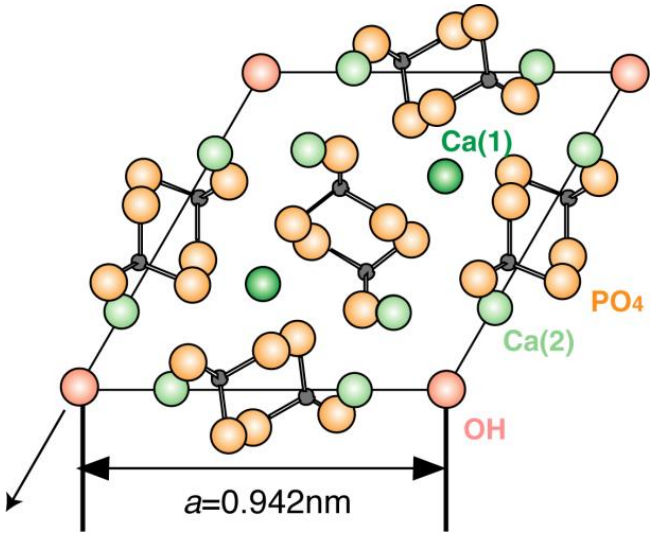

# Identification of phases and crystallinity of powders

International Journal of Materials and Chemistry 2012, 2(1): 19-46
DOI: 10.5923/j.ijmc.20120201.04

**Amorphous Calcium Orthophosphates: Nature, Chemistry and Biomedical Applications**

Sergey V. Dorozhkin

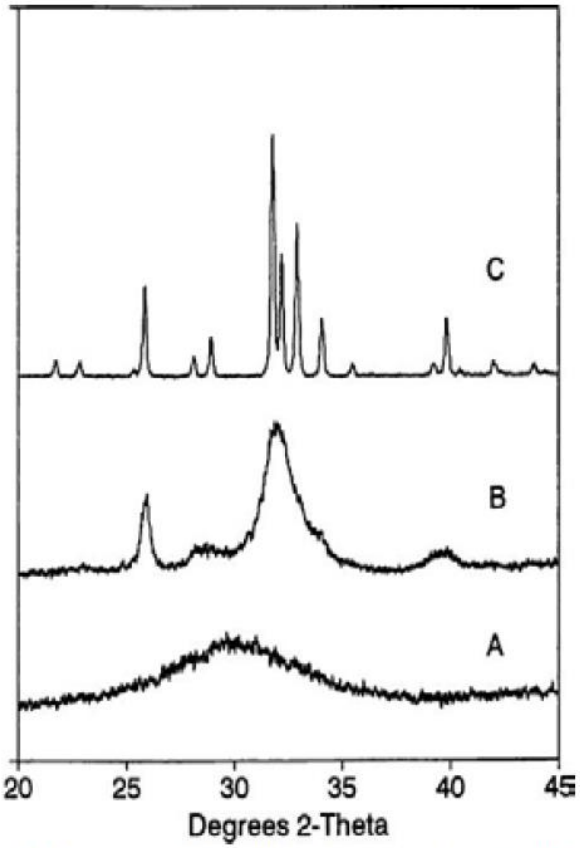


**Figure 2.** Comparison of X-ray diffraction patterns (Cu $K_\alpha$ radiation, = 0.154 nm) of synthetic ACP (bottom), poorly crystalline CDHA (middle) and well crystalline HA (top). The intensity values of the top pattern have been multiplied by a factor of 10, accounting for a high noise level

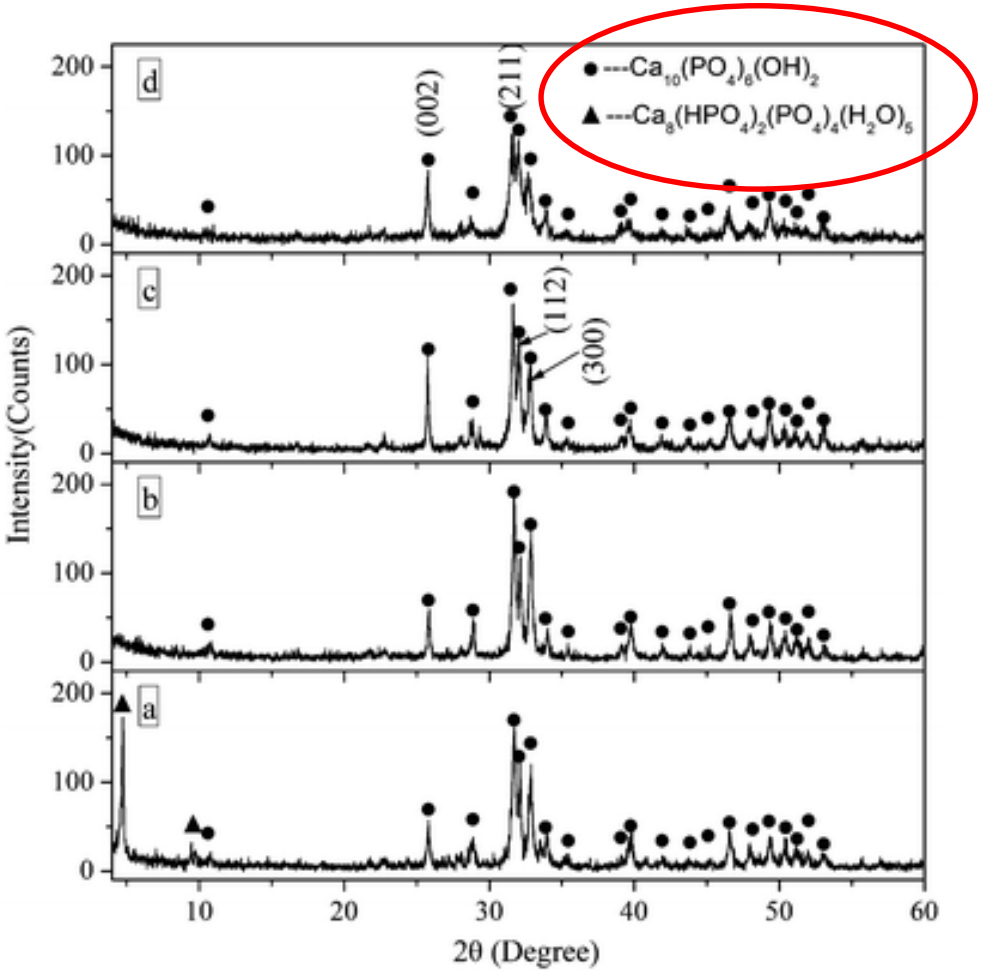


Changlian Chen,[a] Zhiliang Huang,*[a] Wenjuan Yuan,[a] Jianqiu Li,[a] Xiaokun Cheng[a] and Ru-an Chi[a]

Show Affiliations

***CrystEngComm***, 2011, **13**, 1632-1637

# Domain of coherence

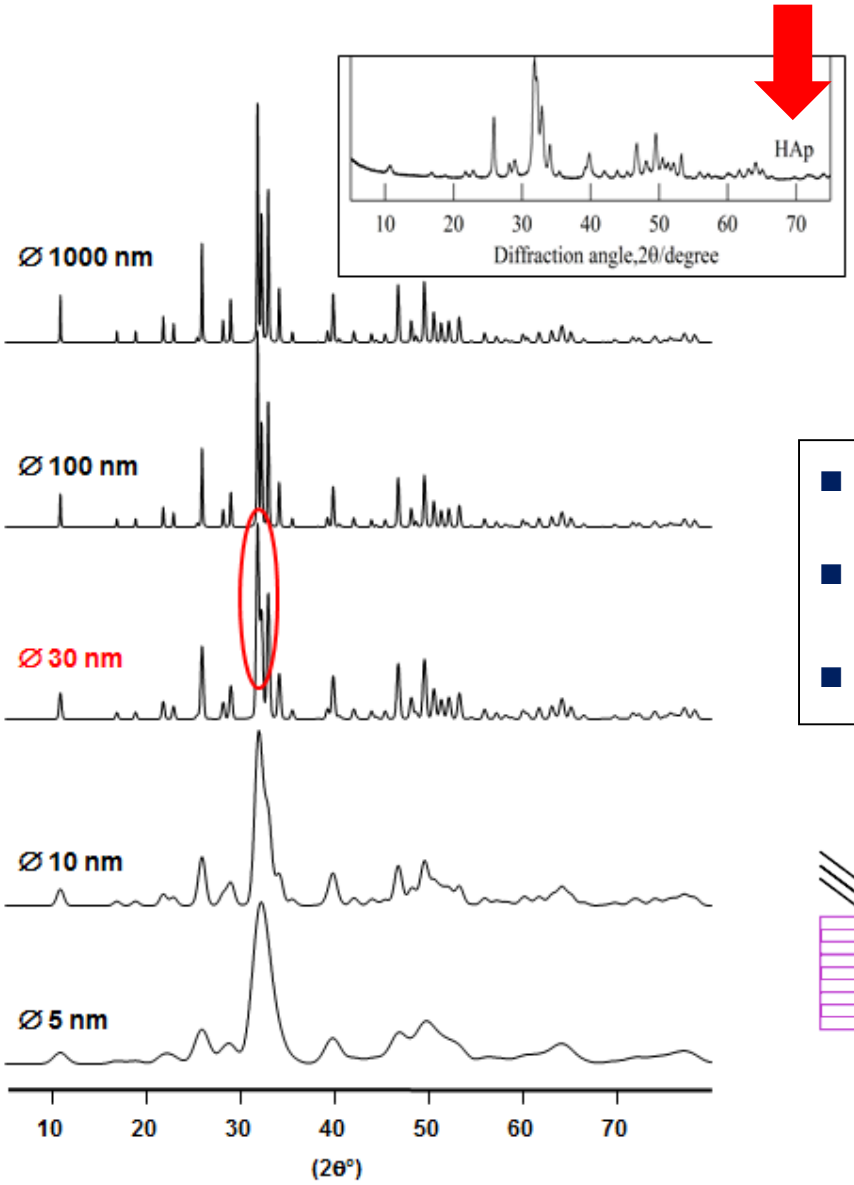


## Scherrer's law

$$B_L = \frac{K\lambda}{L\cos\theta}$$

- chemical disorder
- size of the (nano-) particles
- strain

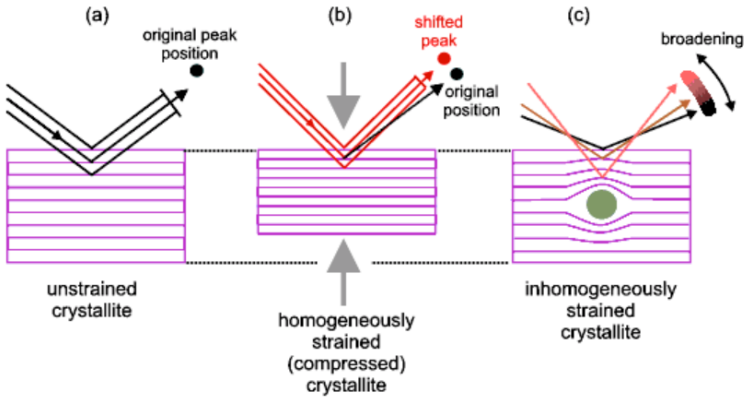

# Neutron diffraction


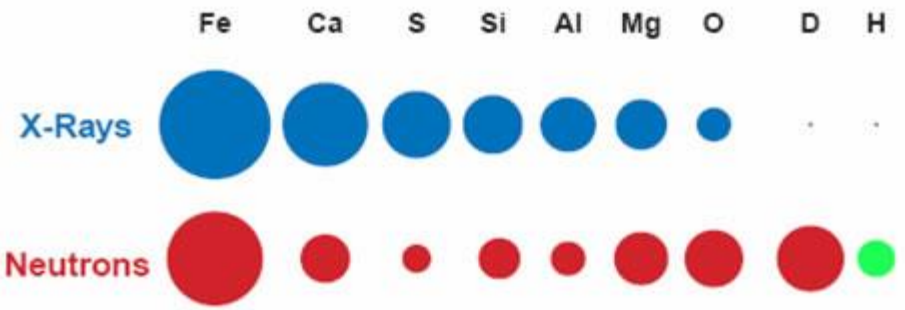


Although superficially similar to x-Ray diffraction, neutron diffraction has many advantages:

- **Contrast.** The neutron scattering strength is not dependent on the atomic number. It is possible to observe the effect of light elements in the presence in heavy ones in the diffraction pattern.
- **Isotopes.** With neutrons the strength of scattering is different for different isotopes so that isotopic substitution can be used to clairy elements of a crystal structure
- **Special Environments.** Neutrons are deeply penetrating so they can diffract off specimens contained in cryo-refrigerators or furnaces, making it easy to examine materials under special conditions and in special environments.
- **Calculable.** Unlike the case for x-Rays, the scattering of neutrons from materials can be accurately calculated making comparison to theoretical.
- **Magnetism.** Neutrons have a magnetic moment and their scattering is sensitive to the magnetic moment of atoms making neutron scattering the ideal means to study magnetic materials.

# Application to hydrated calcium oxalates

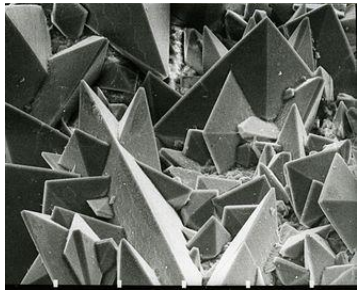

calcium oxalate

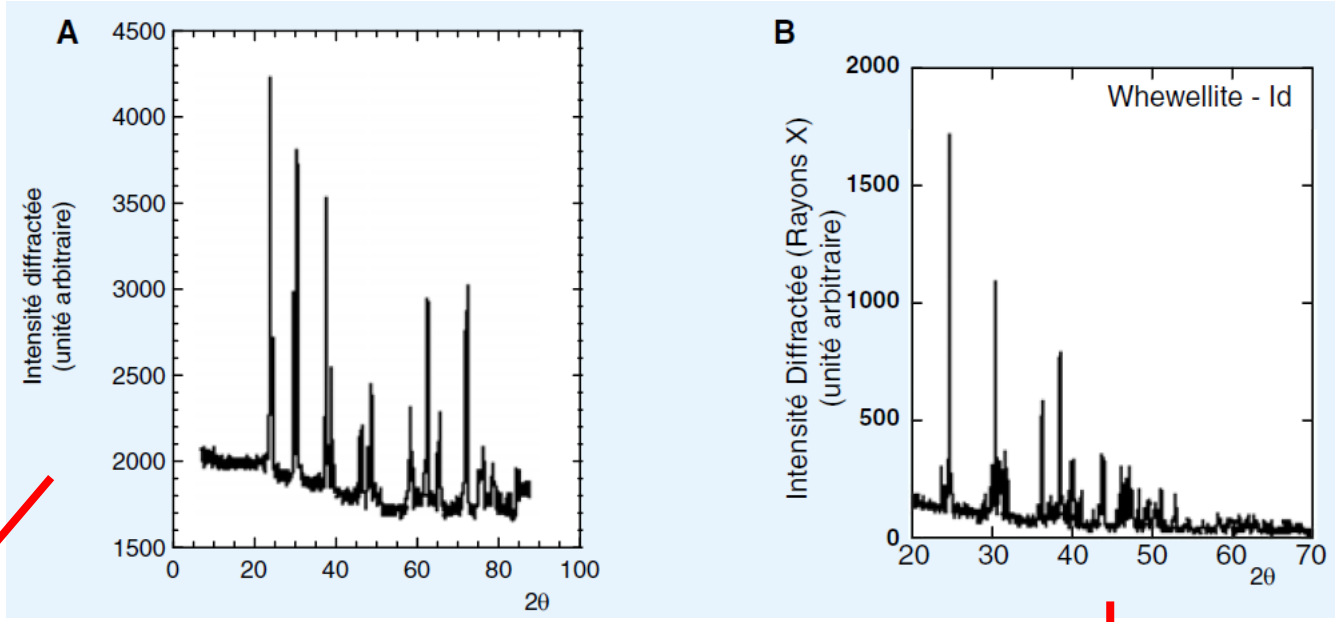


Annales de Biologie Clinique Volume 64, issue 2, Mars-Avril 2006

**Author(s):** D Bazin, M Daudon, P Chevallier, S Rouziere, E Elkaim, D Thiaudiere, B Fayard, E Foy, PA Albouy, G André, G Matzen, E Veron , Laboratoire de physique des solides, Université Paris XI, Orsay, Laboratoire de biochimie A, Hôpital Necker-Enfants Malades, AP-HP, Paris, Laboratoire P. Sue (CEA-CNRS) Saclay, Gif-sur-Yvette, Synchrotron Soleil, L'Orme des Merisiers, Saint-Aubin, Gif-sur-Yvette, Laboratoire Léon Brillouin, CEA-CNRS Saclay, Gif-sur-Yvette, CRMHT-CNRS, Orléans

**powder neutron diffraction**

**powder XRD**

**improved structural models**

# Scanning Electron Microscopy and Transmission Electron Microscopy

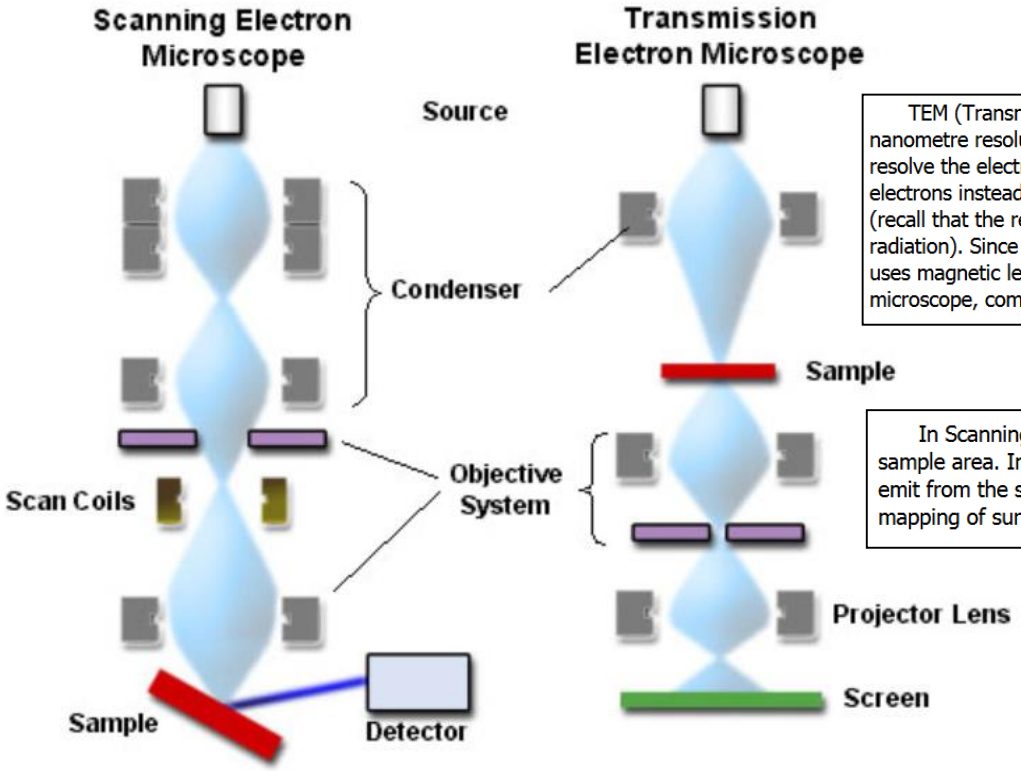


TEM (Transmission Electron Microscopy) allows the visualization of thin slices of material with nanometre resolution. Top of the line instruments have sub-nanometre resolution, and can almost resolve the electron density of individual atoms. A TEM operates much like a light microscope, but uses electrons instead of visible light, since the wavelength of electrons is much smaller than visible light (recall that the resolution limitation of any microscopy is based on the wavelength of the probe radiation). Since electrons are used instead of light, glass lenses are no longer suitable. Instead, a TEM uses magnetic lenses to deflect electrons. Beyond this, a TEM is very similar to a conventional microscope, complete with condenser lenses, objective lenses, and projector lenses.

In Scanning Electron Microscopy (SEM), the electron beam is not projected through the whole sample area. Instead, it is raster-scanned across the surface, and the secondary electrons, or x-rays, emit from the surface are recorded. This generates a lower-resolution image, but allows the direct mapping of surface features, and can even be used for elemental analysis (by study of the x-rays).

- **morphology**
- **diffraction patterns**
- **local chemical analyses**

http://barrett-group.mcgill.ca/tutorials/nanotechnology/nano02.htm

# SEM of bone and derivatives

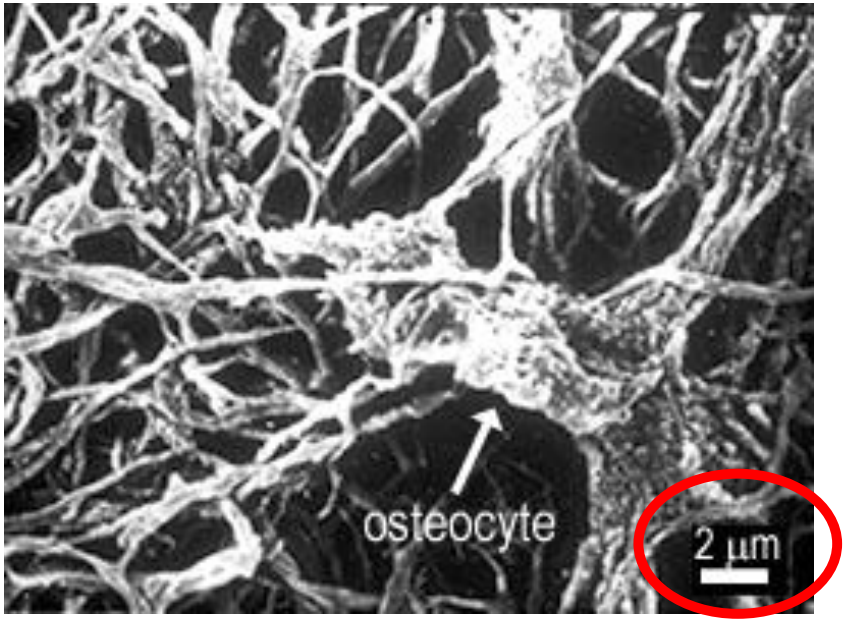


cell in a bone matrix

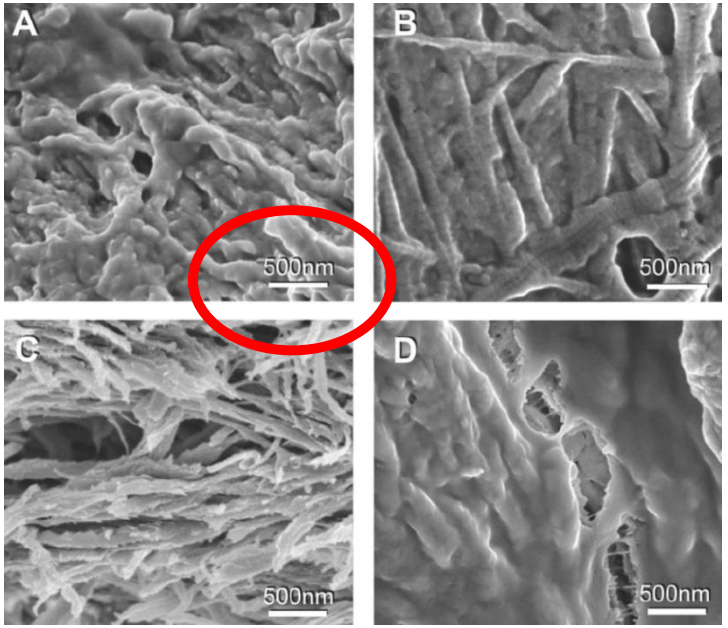


***Figure 5*** *Different morphologies of bone building blocks. Bone is comprised of three basic building blocks - collagen fibrils, mineral plates, and a matrix of unmineralized, non-fibrillar organic material, mostly made of proteoglycans and glycoproteins. (The matrix is also known as the noncollagenous bone matrix). Bone is a highly heterogenous material, partially because it has been adapted to resist different, complex and varying stresses in every species in which it occurs. These scanning electron micrographs show that this heterogenity has its origins in some of the smallest dimensions, as the micrographs were all taken from the same bone sample. They particularly show that the amount of the unmineralized, non-fibrillar organic matrix in trabecular bone varies: A) Fibrils coated with a large amount of non-fibrillar organic material. Particles can still be seen through the smooth cover layer. B) Unmineralized collagen fibrils showing the characteristic 67nm banding pattern. Some particles are between the fibrils but the fibrils are not fully mineralized. C) Mineralized fibrils without non-fibrillar matrix. D) Crack formation in an area with large amounts of non-fibrillar organic matrix. The non-fibrillar organic matrix spans the crack and appears to resist the separation of the mineralized fibrils.*

bone building blocks

# SEM of apatite, calcium oxalates and bioglasses

In vitro

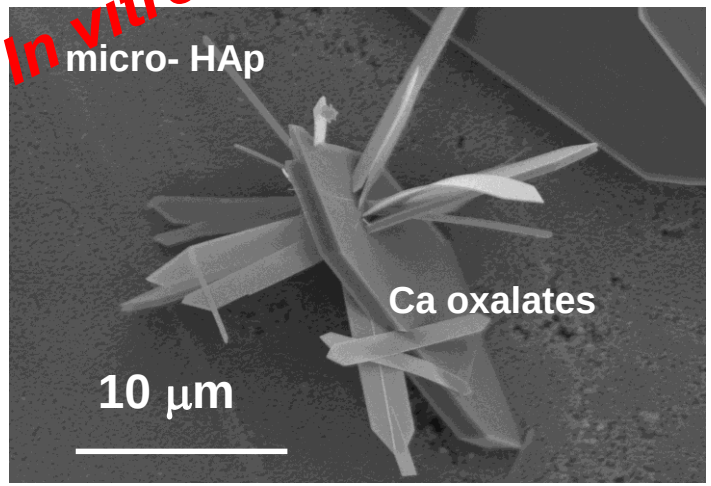


C. Leroy, PhD

C. Chan Chang, Master 2

In vivo


pathological calcifications

(kidney stones & Randall's plaque)

D. Bazin, M. Daudon

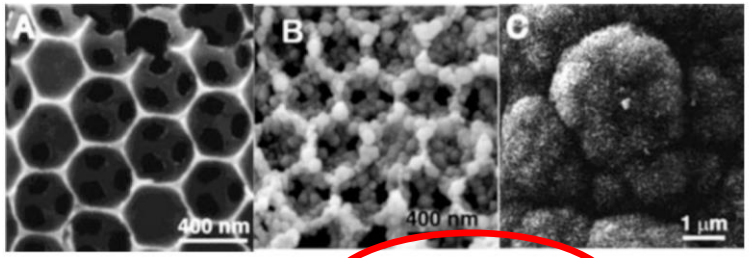


**Fig. 2.9** SEM micrograph of 3D structured macroporous bioglass (**A**) after immersion in simulated biofluids for 3 h (**B**) showing overgrowth of amorphous phosphate on the pore walls and after 4 days (**C**). Reproduced by permission from Chem. Mat. (Yan et al. 2001), Copyright 2001 Am. Chem. Soc.

# TEM of synthetic apatite

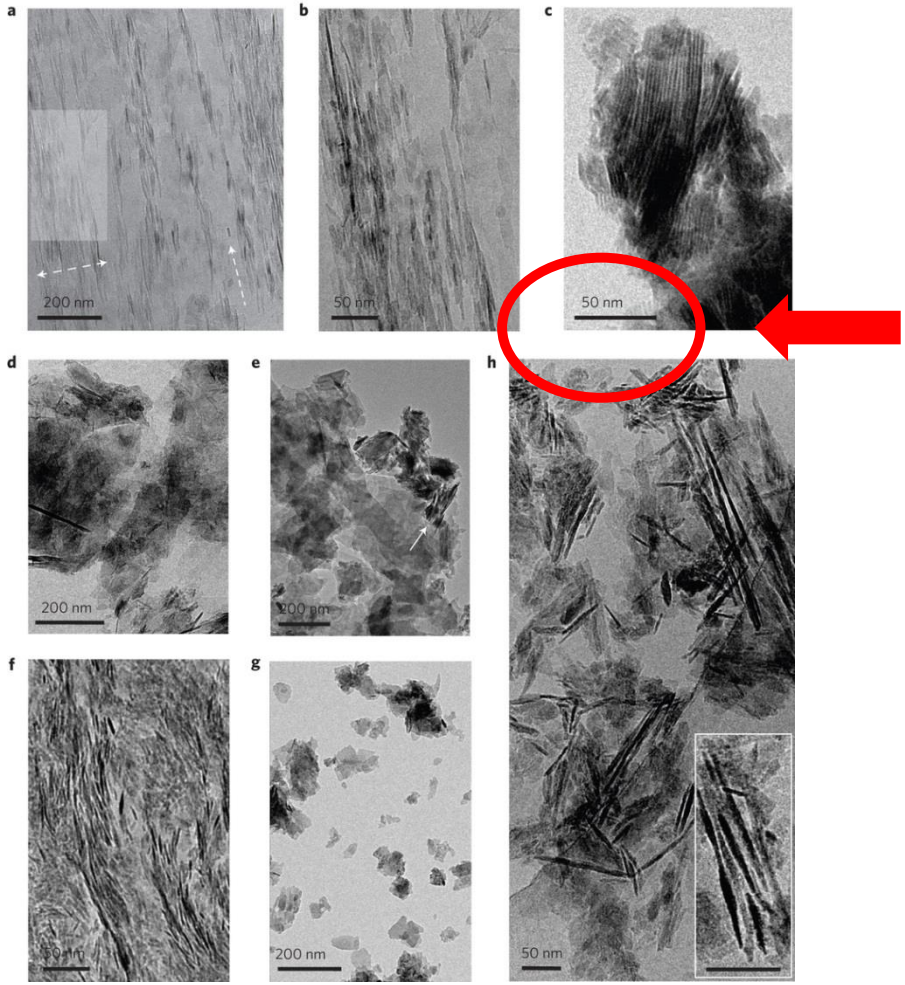


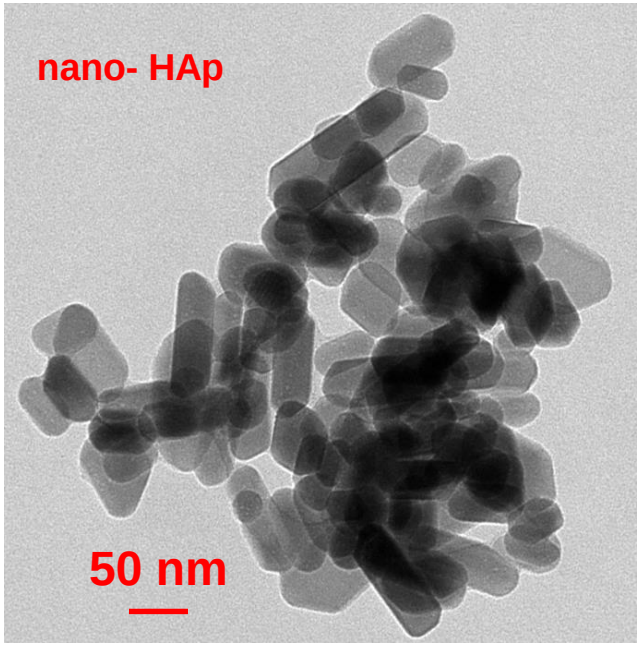


HAp nanoparticles obtained by precipitation methods

Y. Wang *et al*., Nature Mater. 2013

# Atomic Force Microscopy

VOLUME 56, NUMBER 9 PHYSICAL REVIEW LETTERS

## Atomic Force Microscope

G. Binnig[a] and C. F. Quate[b]
*Edward L. Ginzton Laboratory, Stanford University, Stanford, California 94305*
and
Ch. Gerber[c]
*IBM San Jose Research Laboratory, San Jose, California 95193*
(Received 5 December 1985)

The scanning tunneling microscope is proposed as a method to measure forces as small as $10^{-18}$ N. As one application for this concept, we introduce a new type of microscope capable of investigating surfaces of insulators on an atomic scale. The atomic force microscope is a combination of the principles of the scanning tunneling microscope and the stylus profilometer. It incorporates a probe that does not damage the surface. Our preliminary results *in air* demonstrate a lateral resolution of 30 Å and a vertical resolution less than 1 Å.

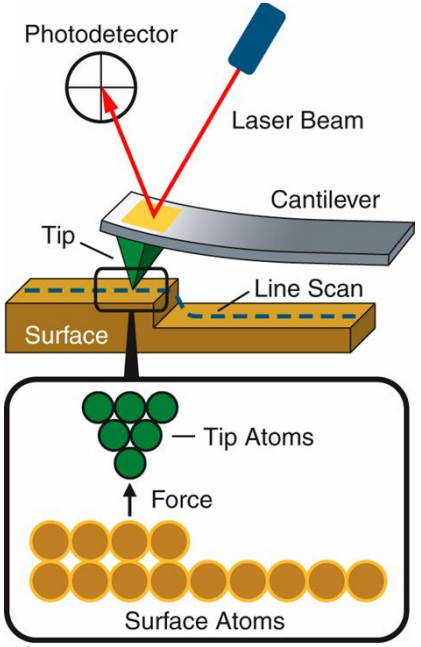


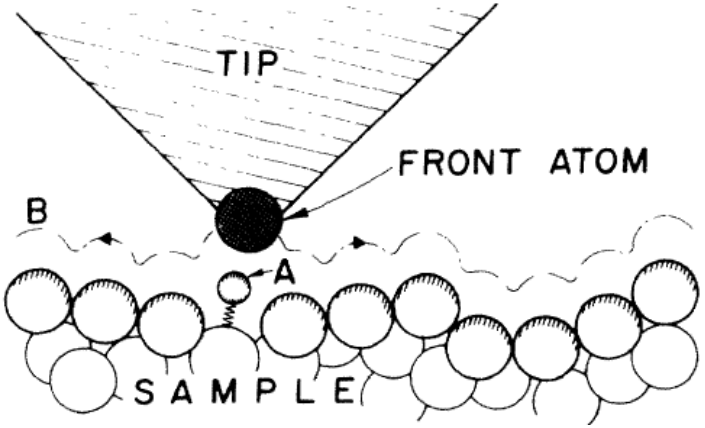


FIG. 1. Description of the principle operation of an STM as well as that of an AFM. The tip follows contour *B*, in one case to keep the tunneling current constant (STM) and in the other to maintain constant force between tip and sample (AFM, sample, and tip either insulating or conducting). The STM itself may probe forces when a periodic force on the adatom *A* varies its position in the gap and modulates the tunneling current in the STM. The force can come from an ac voltage on the tip, or from an externally applied magnetic field for adatoms with a magnetic moment.

# Analysis of surfaces

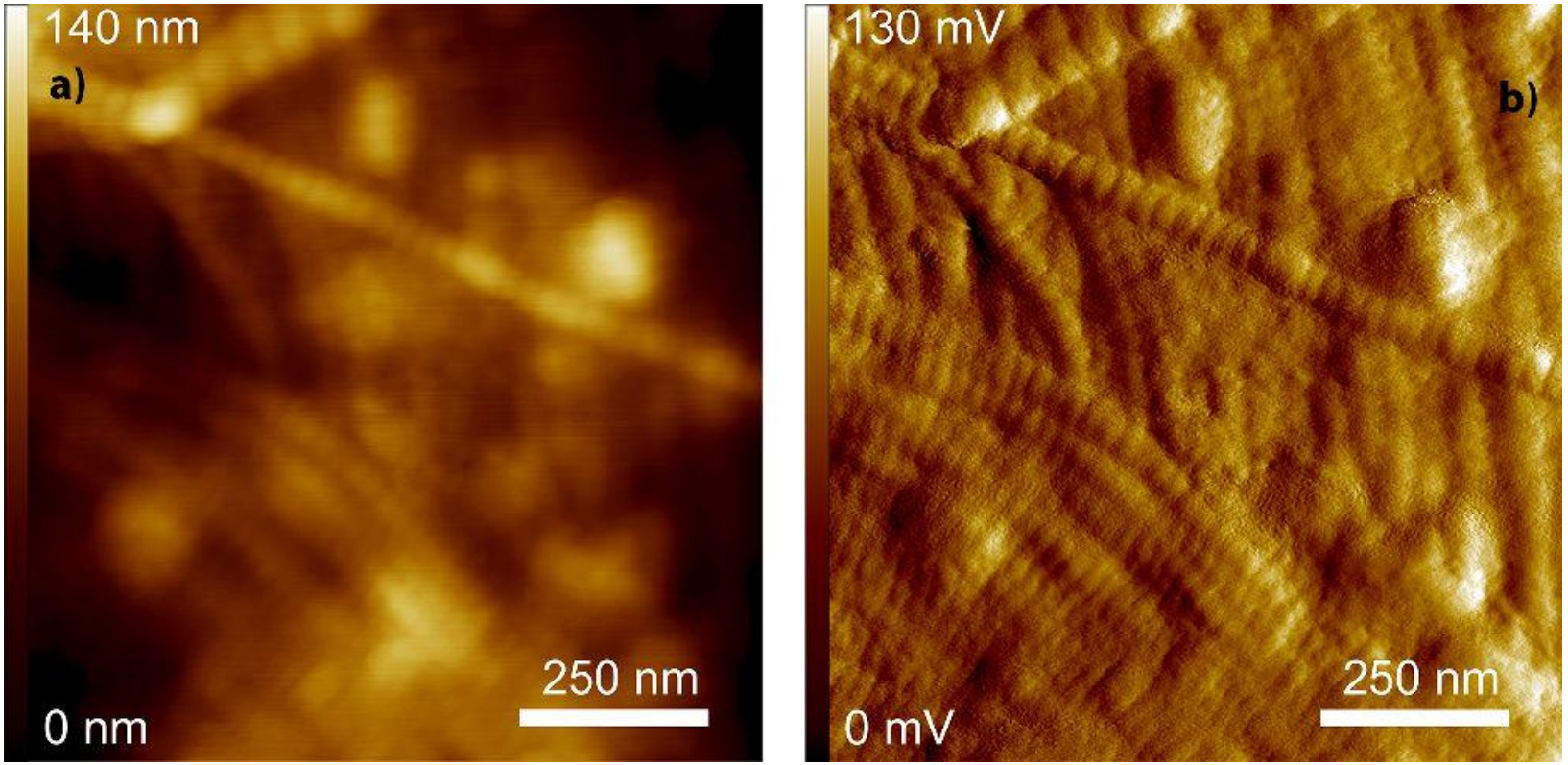


Figure 8 AFM topography and amplitude images of collagen found in the histological skin sample of Zweeloo Woman. Figure (left) shows collagen fibrils (measuring 2 x 2 µm) with their characteristic banding pattern. The fibrils form a network-like structure. Some of them overlap one another. The contours of the fibrils are faint. The amplitude image (right) shows the fibril contours in more detail.

# Cell on surfaces

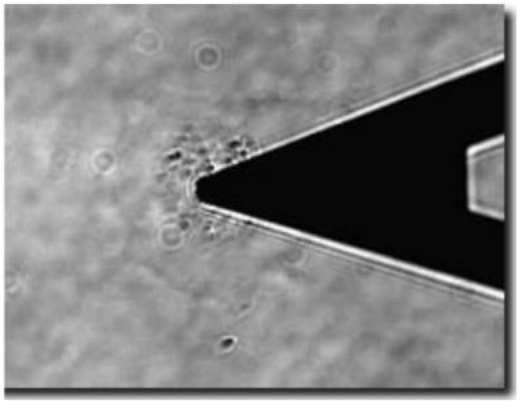

AFM Probe Tip Indenting an Osteoblast

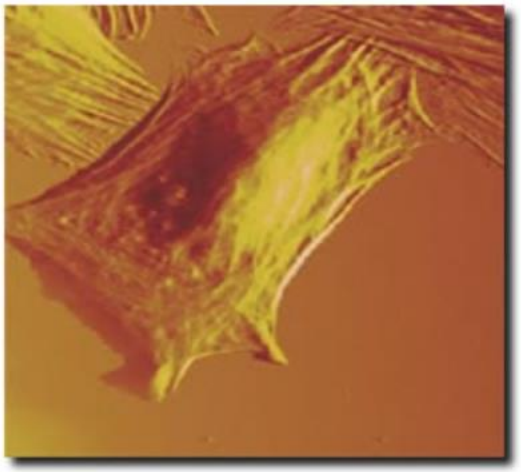

AFM Imaging Mode: Osteoblast Adhered to Fibronectin Coated Surface


*Related Publications*

1. Takai, E., Katz, R. W., Landesberg, R., Hung, C. T., and Guo, X. E. Adhesion Strength, Focal Adhesion Kinase Activation, and Cytoskeletal Organization of Osteoblasts on Various Substrates, Trans. 48th Orthopaedic Research Society Annual Meeting, 27:535, Dallas, TX, Feb. 10-13, 2002. Download
2. Guo, X. E., Shyu, J., Takai, E., Hung, C. T. and Costa, K. D. Substrates Influence Osteoblast Elastic Modulus Measured by Atomic Force Microscopy, Trans. 48th Orthopaedic Research Society Annual Meeting, 27:521, Dallas, TX, Feb. 10-13, 2002. Download

# Applications of the synchrotron radiation

**see:** Annales de Biologie Clinique Volume 64, issue 2, Mars-Avril 2006

**Author(s):** D Bazin, M Daudon, P Chevallier, S Rouziere, E Elkaim, D Thiaudiere, B Fayard, E Foy, PA Albouy, G André, G Matzen, E Veron , Laboratoire de physique des solides, Université Paris XI, Orsay, Laboratoire de biochimie A, Hôpital Necker-Enfants Malades, AP-HP, Paris, Laboratoire P. Sue (CEA-CNRS) Saclay, Gif-sur-Yvette, Synchrotron Soleil, L'Orme des Merisiers, Saint-Aubin, Gif-sur-Yvette, Laboratoire Léon Brillouin, CEA-CNRS Saclay, Gif-sur-Yvette, CRMHT-CNRS, Orléans

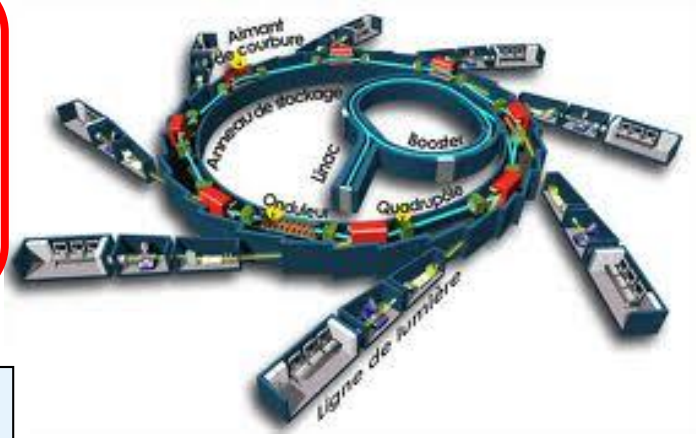


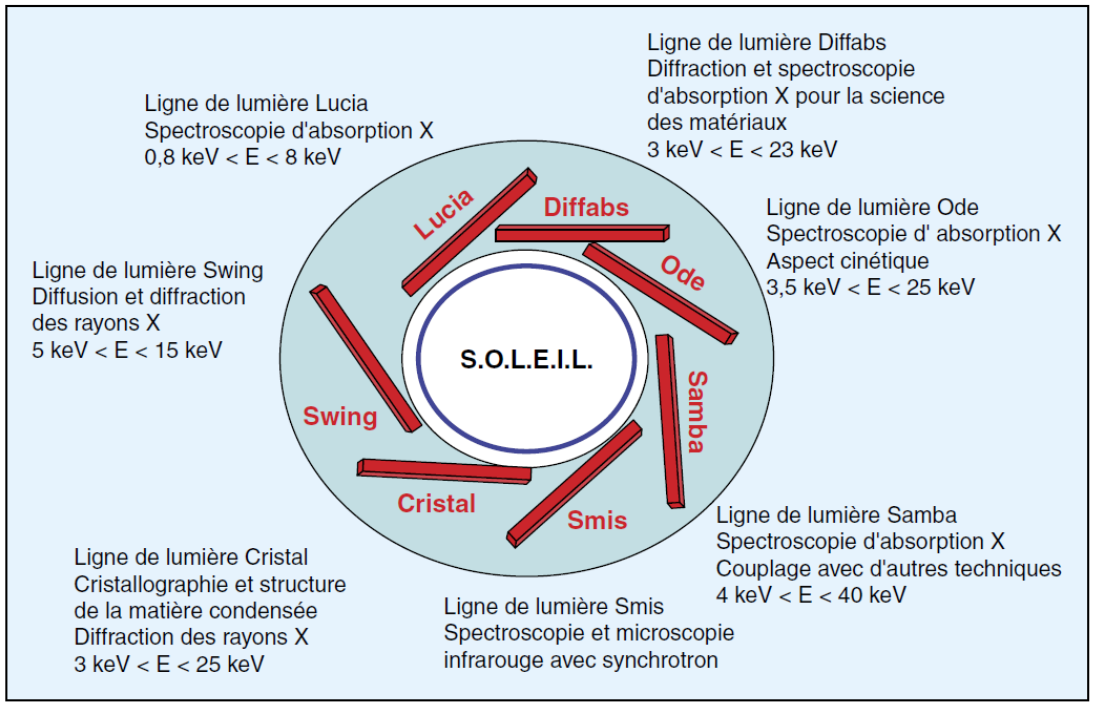


# A large variety of experiments

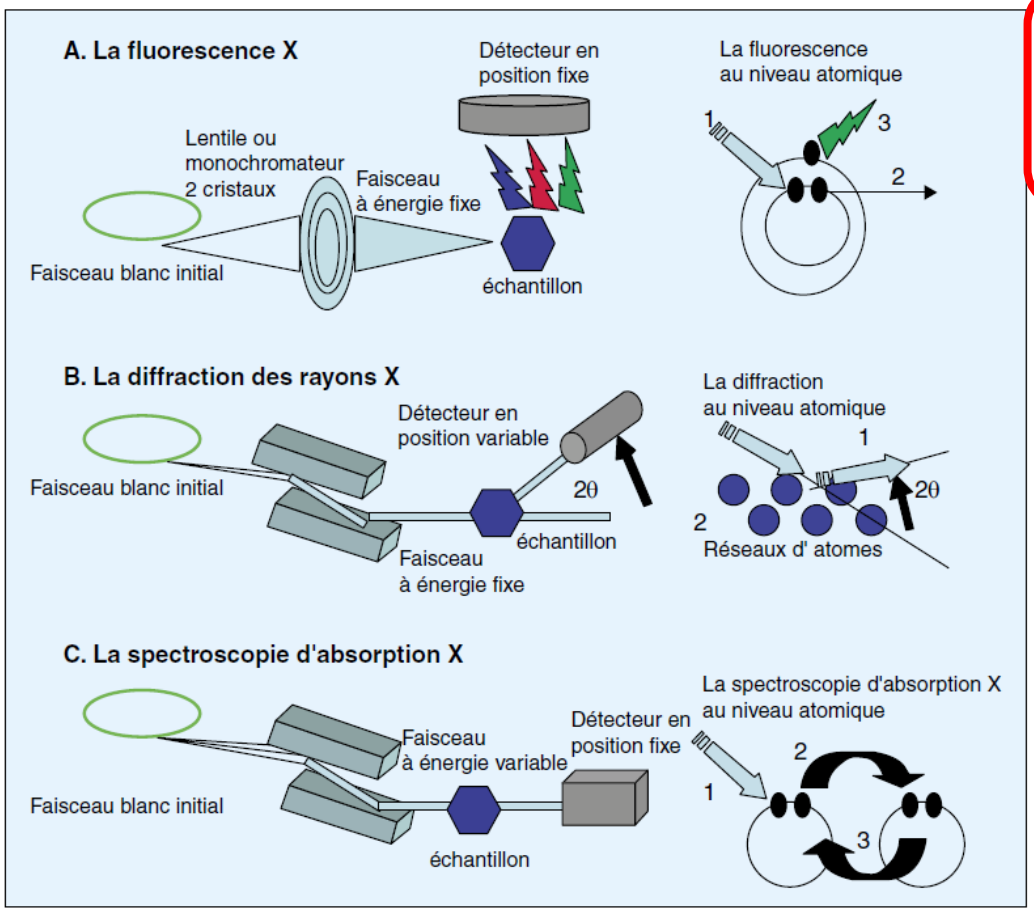


see: Annales de Biologie Clinique Volume 64, issue 2, Mars-Avril 2006

**Author(s):** D Bazin, M Daudon, P Chevallier, S Rouziere, E Elkaim, D Thiaudiere, B Fayard, E Foy, PA Albouy, G André, G Matzen, E Veron , Laboratoire de physique des solides, Université Paris XI, Orsay, Laboratoire de biochimie A, Hôpital Necker-Enfants Malades, AP-HP, Paris, Laboratoire P. Sue (CEA-CNRS) Saclay, Gif-sur-Yvette, Synchrotron Soleil, L'Orme des Merisiers, Saint-Aubin, Gif-sur-Yvette, Laboratoire Léon Brillouin, CEA-CNRS Saclay, Gif-sur-Yvette, CRMHT-CNRS, Orléans

**Figure 2. A.** Schéma de principe d'un montage de fluorescence X. Le faisceau incident blanc est envoyé sur une lentille de Bragg Fresnel qui le convertit en faisceau monochromatique avec une énergie de 18 KeV et le focalise sur l'échantillon. Les photons émis sont ensuite collectés par le détecteur en silicium dopé au lithium. Au niveau atomique, le faisceau monochromatique (1 en *figure 2A*) éjecte un électron de cœur (2 en *figure 2A*). En mode radiatif, la désexcitation s'effectue par émission de photons de fluorescence (3 en *figure 2A*). **B.** Schéma de principe d'un montage de diffraction X (le faisceau incident blanc est monochromatisé par un montage "deux cristaux". Un détecteur vient mesurer le faisceau diffracté dont l'énergie est celle du faisceau incident. Au niveau atomique, le faisceau monochromatique est diffracté (1 en *figure 2B*) par le réseau d'atomes (2 en *figure 2B*). Un angle $2\theta$ est défini entre le faisceau incident et le faisceau diffracté. **C.** Schéma de principe d'un montage de spectroscopie d'absorption X. Le faisceau incident blanc est monochromatisé par un montage "deux cristaux". Un détecteur vient mesurer l'absorption due à la traversée du faisceau par l'échantillon. En modifiant l'énergie du faisceau incident, on construit le spectre d'absorption de l'échantillon. Au niveau atomique, le faisceau monochromatique (1 en *figure 2C*) éjecte un électron de cœur (2 en *figure 2C*). Celui-ci va se réfléchir sur les atomes voisins (3 en *figure 2C*). C'est ce processus de réflexion de l'électron qui donne lieu aux variations du coefficient d'absorption qui sont mesurées lorsque l'on modifie l'énergie du faisceau incident.

# X ray absorption

**X-ray Absorption Near Edge Spectroscopy**

**Extended X-ray Absorption Fine Structure**

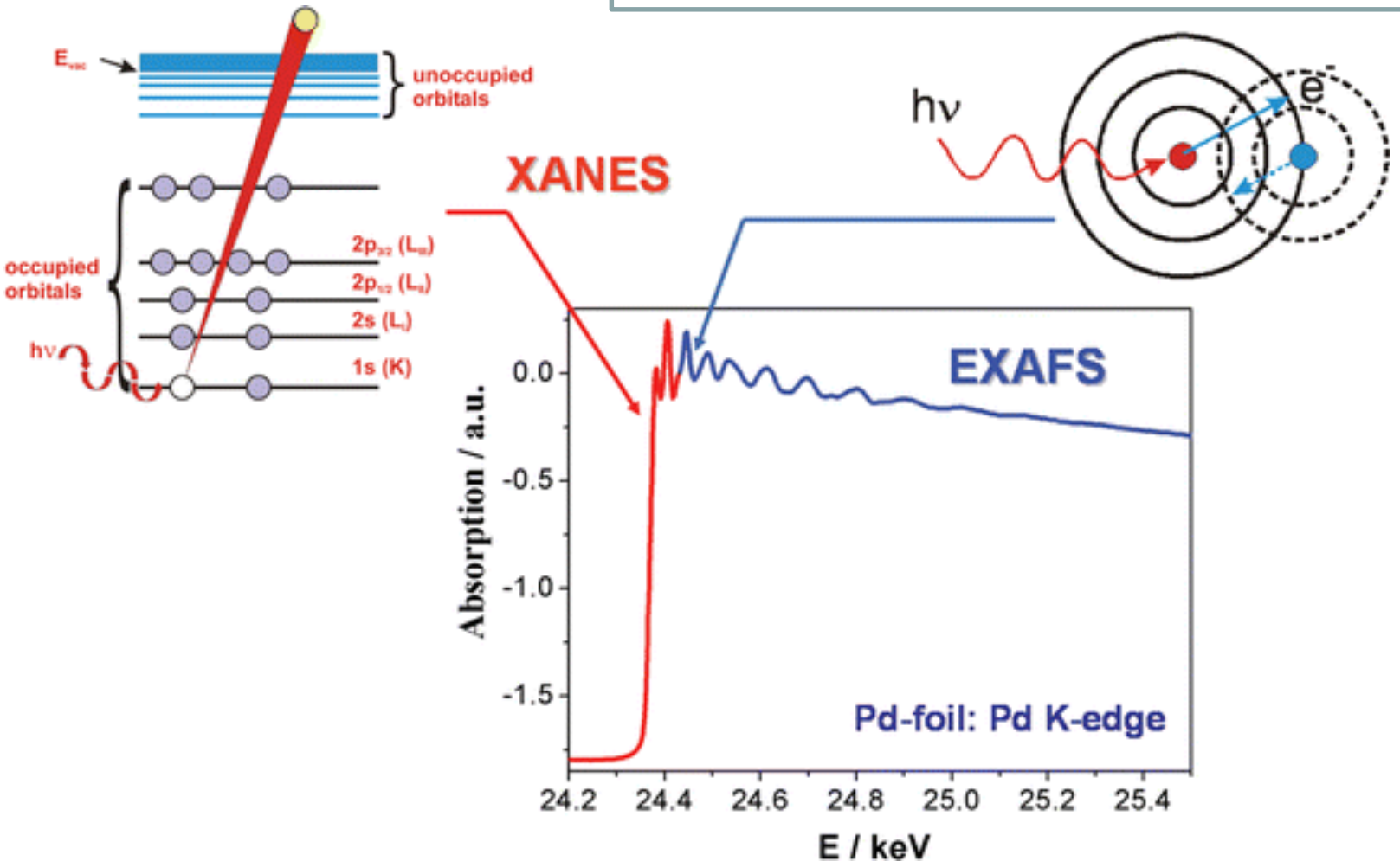


**the (linear) absorption coefficient of X-rays by an element**

# X ray absorption

**X-ray Absorption Near Edge Spectroscopy**

**Extended X-ray Absorption Fine Structure**

**XANES:**

- **oxydation state**
- **site symmetry**

**carefull calibration of the E scale**

**error bar for accurate comparison of XANES spectra**

**EXAFS:**

- **type of ligands**
- **distances**
- **coordination number**

**distances:** 0.02 Å

**CN:** 20-25%

$\chi(E)$ or $\chi(k)$

$$k = \frac{2\pi}{\lambda} = \sqrt{\frac{2m_e(E - E_0)}{\hbar^2}}$$

electron mass

photoelectron wavenumber

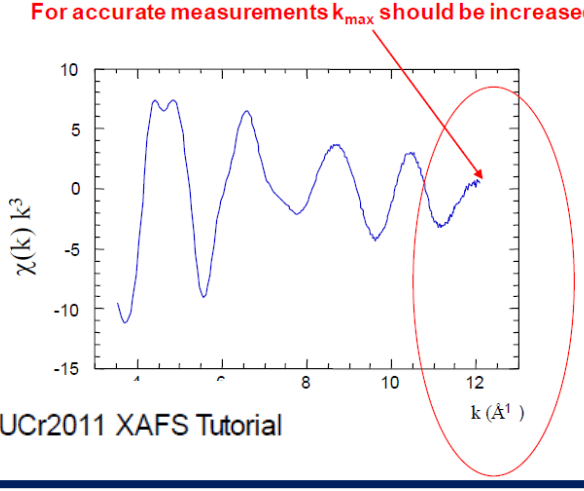


I. Ascone-IUCr2011 XAFS Tutorial

# Fe containing samples

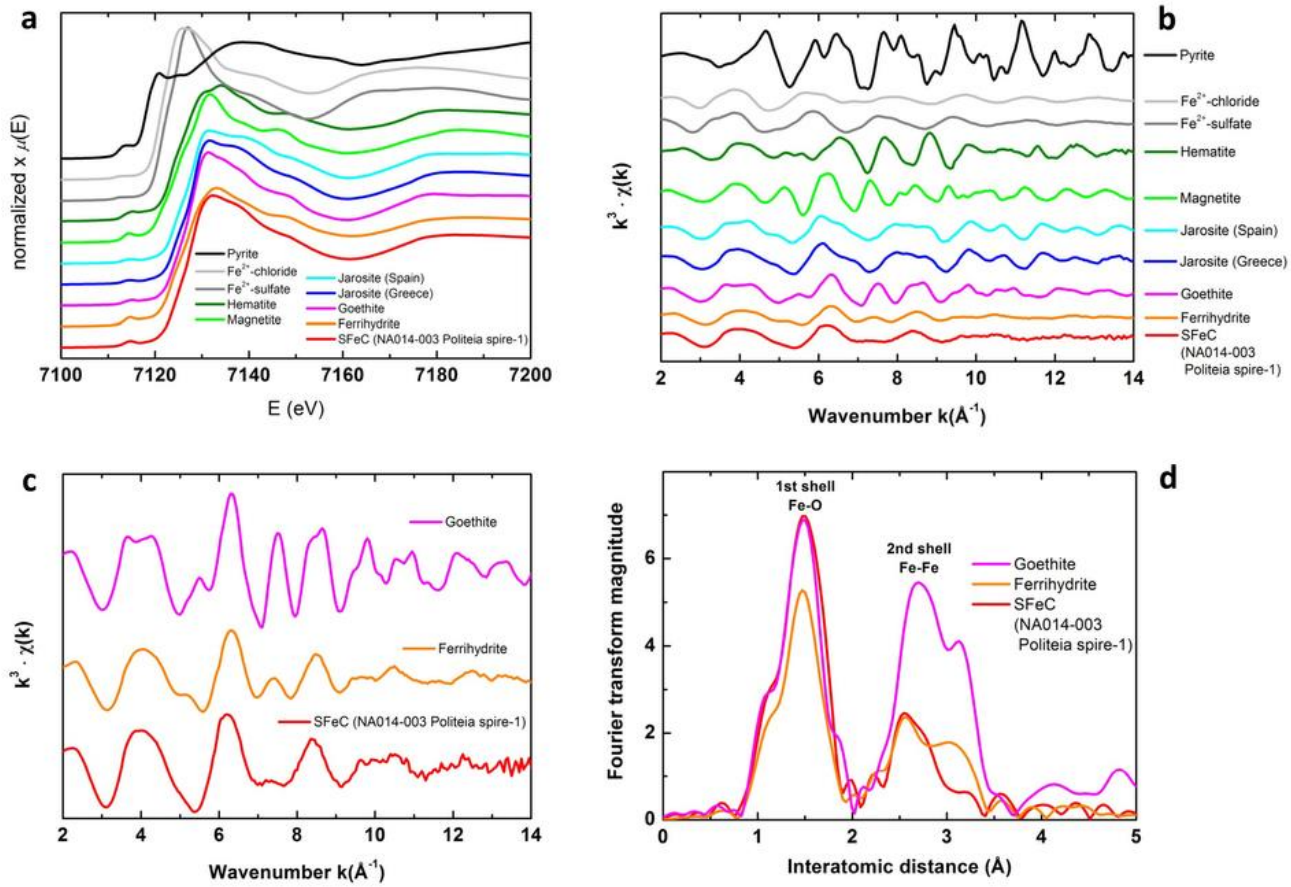


From

**New insights into hydrothermal vent processes in the unique shallow-submarine arc-volcano, Kolumbo (Santorini), Greece**

**Stephanos P. Kilias, Paraskevi Nomikou, Dimitrios Papanikolaou, Paraskevi N. Polymenakou, Athanasios Godelitsas, Ariadne Argyraki, Steven Carey, Platon Gamaletsos, Theo J. Mertzimekis, Eleni Stathopoulou, Joerg Goettlicher, Ralph Steininger, Konstantina Betzelou, Isidoros Livanos, Christos Christakis, Katherine Croff Bell & Michael Scoullos**

*Scientific Reports* **3**, Article number: 2421 | doi:10.1038/srep02421

Received 26 February 2013 | Accepted 23 July 2013 | Published 13 August 2013

# Applications to the study of KS

**see:** Annales de Biologie Clinique Volume 64, issue 2, Mars-Avril 2006

**Author(s):** D Bazin, M Daudon, P Chevallier, S Rouziere, E Elkaim, D Thiaudiere, B Fayard, E Foy, PA Albouy, G André, G Matzen, E Veron , Laboratoire de physique des solides, Université Paris XI, Orsay, Laboratoire de biochimie A, Hôpital Necker-Enfants Malades, AP-HP, Paris, Laboratoire P. Sue (CEA-CNRS) Saclay, Gif-sur-Yvette, Synchrotron Soleil, L'Orme des Merisiers, Saint-Aubin, Gif-sur-Yvette, Laboratoire Léon Brillouin, CEA-CNRS Saclay, Gif-sur-Yvette, CRMHT-CNRS, Orléans

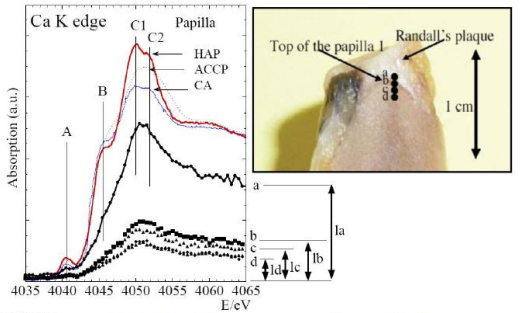


Figure 2. Left: XANES part of the absorption spectra for the papilla 1 and reference compounds. Right: The RP can be clearly seen as the white part at the top of the renal papilla. a, b, c and d refer to acquisition points related to X-ray absorption experiments.

**M. Daudon[1] and D Bazin[2,3]**

[1]APHP, Hôpital Tenon, Service des Explorations Fonctionnelles, 4 rue de la Chine, 75970 Paris cedex 20, France
[2]Laboratoire de Chimie de la Matière Condensée de Paris, UPMC et Collège de France, France
[3]CNRS, Laboratoire de Physique des Solides, UPS, 91405 Orsay, France

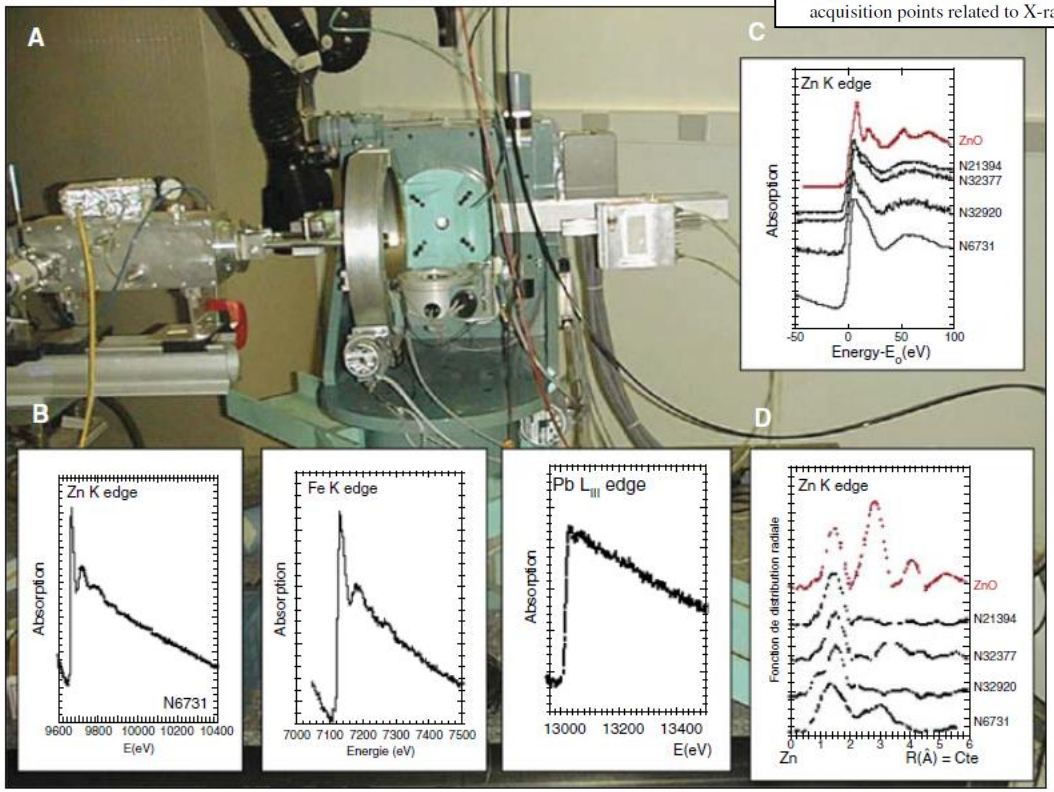


**Figure 5. A.** Photographie du montage de la ligne de lumière DiffAbs qui sera implantée sur SOLEIL. **B.** Spectre d'absorption de différents éléments lourds (Zn, Fe, Pb) mis en évidence dans des calculs rénaux. La spectroscopie d'absorption X permet une détermination de l'ordre local autour de chacun de ces éléments. **C.** Seuil d'absorption d'un spectre d'absorption collecté au seuil du zinc. **D.** Fonction de distribution radiale autour du zinc. Le premier pic est associé aux liaisons ZnO, le second massif aux atomes situés au-delà des atomes d'oxygène entourant l'atome de zinc.

# Micro-tomography

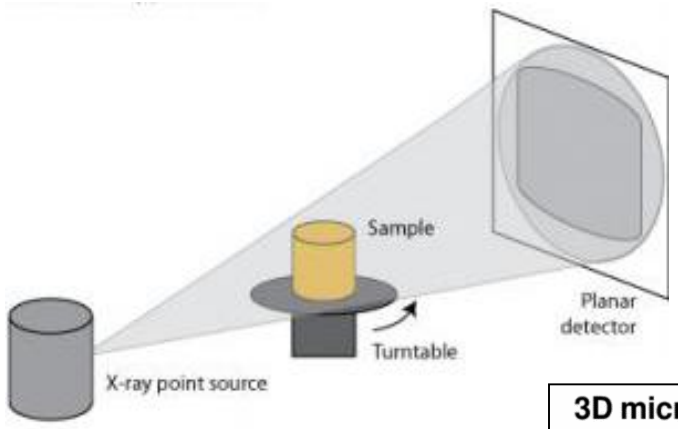


**3D micro-computed tomography of trabecular and cortical bone architecture with application to a rat model of immobilisation osteoporosis**

A. Laib[1] O. Barou[2] L. Vico[2] M. H. Lafage-Proust[2] C. Alexandre[2] P. Rügsegger[1]

[1]Institute for Biomedical Engineering, University of Zürich and Swiss Federal Institute of Technology (ETH), Zürich, Switzerland
[2]Laboratory of Bone Biology and Biochemistry, Saint-Etienne University, Saint-Etienne, France

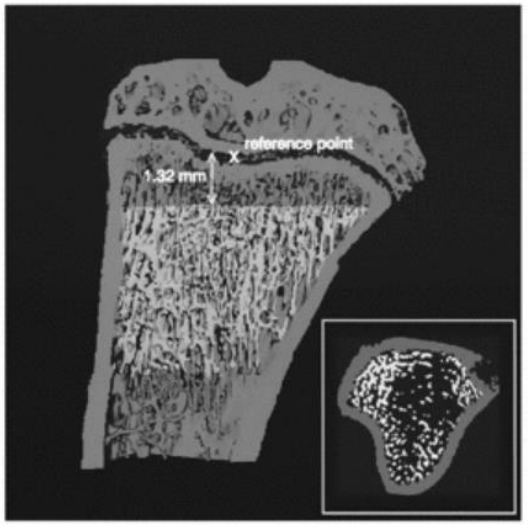


**Fig. 1** *Cut through the 3D image of a MicroCT measurement of a control rat. The conforming VOI is highlighted. The reference point at the end of the epiphysis is shown as a cross, from which the conforming region starts at a fixed distance of 1.32 mm. The inset shows a transaxial cut through the bone with the VOI highlighted*

**X-ray Computed Tomography is a nondestructive technique for visualizing interior features within solid objects, and for obtaining digital information on their 3D geometries and properties.**

This technique combines 2D radiography with a numerical technique known as 3D reconstruction to precisely characterize the internal microstructure of a wide range of materials. The resulting 3D volume is made up a series of slices corresponding to what the object being scanned would look like if it were sliced along the cross-sectional plane, and correspond to a certain thickness of the object being scanned. So, while a digital image is compsed of pixels, a tomographic image is composed of voxels. The gray levels in a tomographic image correspond to X-ray attenuation, which reflects the proportion of X-rays scattered or absorbed as they pass through each voxel. X-ray attenuation is primarily a function of X-ray energy and the density and composition of the material being imaged.

The tomography technique has the potential to transform research in materials science and engineering by observing in 3D the real shape and connectivity of microstructure and defects under different processing conditions, as well as developing numerical models based on realistic 3D geometry.

# Mechanical properties

UNIVERSITY OF CAMBRIDGE

DoITPoMS

Home | Teaching & Learning Packages | Lecture Demonstration Packages | Micrographs | Videos | Learn more...

DoITPoMS › TLP Library › Structure of bone and implant materials › Mechanical properties of bone

- Home
- Aims

## Mechanical properties of bone

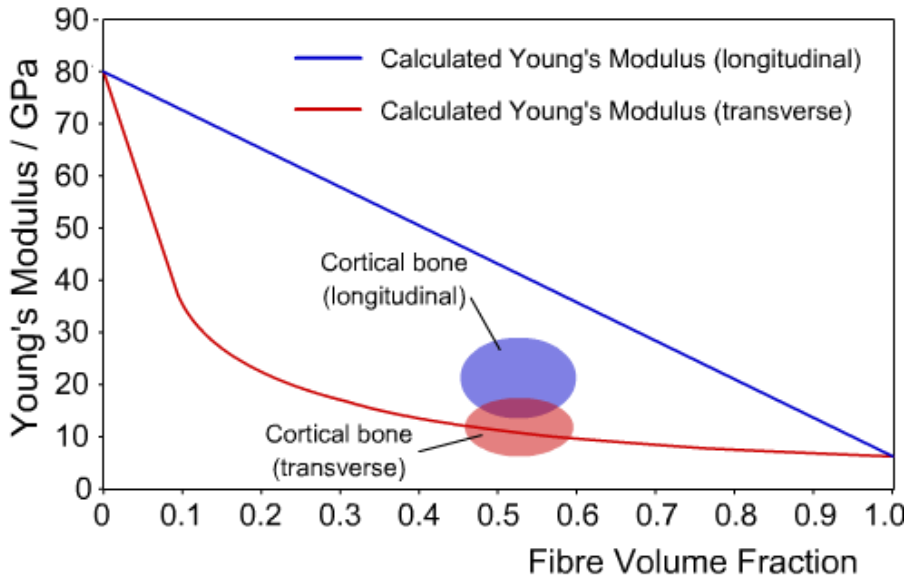


**Crack propagation in cortical bone**

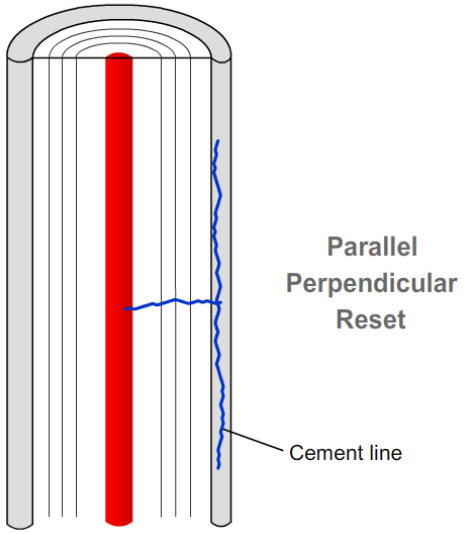


Perpendicular cracks change direction on reaching the cement line, spreading out parallel to the osteon direction.

# Thermal analyses

JOURNAL OF MATERIALS SCIENCE 38 (2003) 4777–4782

## Thermal analysis study of human bone

L. F. LOZANO, M. A. PEÑA-RICO, A. HEREDIA
*Instituto de Física, Universidad Nacional Autónoma de México, Apartado Postal 20-364, 01000 México D.F., México*

J. OCOTLÁN-FLORES
*Centro de Instrumentos, UNAM, Apartado Postal 70-186, Mexico D.F., México*

A. GÓMEZ-CORTÉS
*Instituto de Física, Universidad Nacional Autónoma de México, Apartado Postal 20-364, 01000 México D.F., México*

R. VELÁZQUEZ
*Centro de Física Aplicada y Tecnología Avanzada, UNAM, Apdo. Postal 1-1010 Querétaro, Qro. 76000, México*

I. A. BELÍO
*Escuela de Odontología, Universidad Autónoma de Sinaloa, Blvd. de Las Américas y Universitarios, C.P. 80010 Culiacán, Sinaloa, México*

L. BUCIO*
*Instituto de Física, Universidad Nacional Autónoma de México, Apartado Postal 20-364, 01000 México D.F., México*
*E-mail: bucio@fisica.unam.mx*

We have studied the thermal stability of human bone tissue and also its bone-extracted type-I collagen. We have used differential thermal analysis (DSC), infrared spectroscopy (FTIR) and gas chromatography. For type-I Collagen, variations of an exothermic maximum peak were observed between 500 and 530°C depending on the extraction method. These variations are related to high thermal stability of extracted collagen as opposed to thermal stability found in bone tissue, which maximum exothermic peak was found at ≈350°C. Total combustion enthalpy $\Delta H$ values are similar: $-8.4 \pm 0.11$ kJ/g for bone tissue, and between $-7.9$ to $-8.9$ kJ/g in extracted collagen (depending on the extracting method). These findings, along with the results obtained by infrared spectroscopy and chromatographic techniques, demonstrate that the loss of thermal stability in type I collagen is due to its interactions with carbonate hydroxyapatite nanocrystals. The interactions cause a change in the molecular properties of collagen during mineralization, (specifically in its cross-links and other chemical interactions) which have an effect on fiber elasticity and on strength of bone tissue as a whole. We discuss the decomposition/combustion process and also how calorimetric measurement affects specific interactions between mineral and organic phases. 

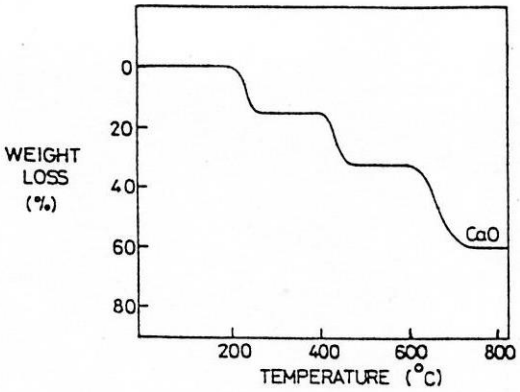


Fig. 2. Courbe d'analyse thermogravimétrique d'un oxalate de calcium hydraté.

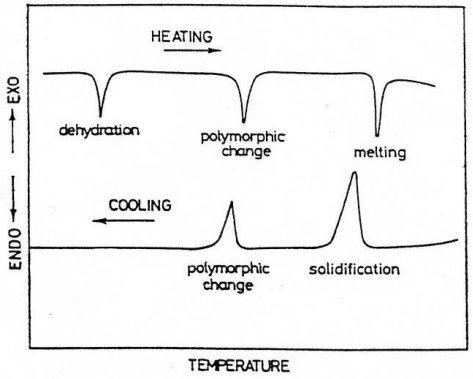


Fig. 21. ATD schématiques de phénomènes réversibles et irréversibles.